We are IntechOpen, the world's leading publisher of Open Access books Built by scientists, for scientists

4,800
Open access books available

122,000
International authors and editors

135M
Downloads

Our authors are among the

154
Countries delivered to

TOP 1%
most cited scientists

12.2%
Contributors from top 500 universities

CLARIVATE ANALYTICS BOOK CITATION INDEX INDEXED

WEB OF SCIENCE™

Selection of our books indexed in the Book Citation Index in Web of Science™ Core Collection (BKCI)

Interested in publishing with us?
Contact book.department@intechopen.com

Numbers displayed above are based on latest data collected.
For more information visit www.intechopen.com

Chapter 10

Utilization of Compounds of Phosphorus

Petr Ptáček

Additional information is available at the end of the chapter

http://dx.doi.org/10.5772/62217

Abstract

The last chapter of this book provides brief description of utilization of apatites and phosphorus-bearing compounds in industry and material science research. Since the chemistry of phosphorus is quite complicated and a quickly developing field of science, the topics described below are only limited insights to chemically bonded ceramics and refractories, dental phosphate cements, oil-well cements, phosphate glasses and glass ceramics. Chapter continues with description of functional phosphate materials applied as solid oxide fuel cells electrolytes, sensors, phosphors, catalysts and coatings. The chapter ends with introduction of basic ideas for biological apatite in bone tissue engineering, collagen apatite composites, apatite layers and biocoatings.

Keywords: Apatite, Chemically Bonded Ceramics, Phosphate Cement, SFOC Electrolytes, Sensors, Biological Apatite, Collagen, Biocoatings

In the previous chapter, the utilization of phosphate ore was described. Elemental phosphorus (**Section 9.1**) and phosphoric acid (**Section 9.2**) are used in the manufacturing of other phosphorus compounds (as illustrated in **Fig. 1**) and materials, which are briefly reported in this chapter. Since the chemistry of phosphorus is quite complicated and a quickly developing field of science, the topics described below are only limited insights to phosphorus-bearing compounds utilized in the industry and material science research.

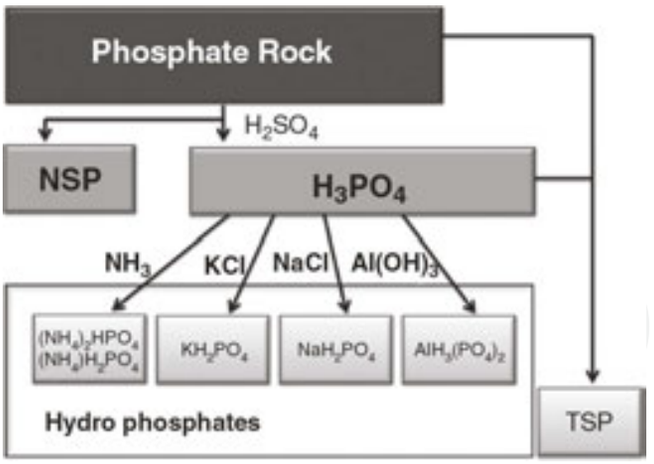

Fig. 1. Flow chart of production of acid phosphates from phosphate ores [1].

10.1. Chemically bonded phosphate ceramics

Ceramics are formed by the compaction of powders and their subsequent fusion at high to very high temperatures, ranging somewhere from ~700° to 2000°C. Once fused, the resulting ceramics are hard and dense and exhibit very good corrosion resistance [2]. Among the conventional ceramic bonds, the chemical (organic and inorganic) and hydraulic bonds were used during the preparation of ceramic materials.

Phosphate bond can be utilized for the preparation of hard and quick-setting ceramic materials, chemically bonded phosphate ceramics (PCBC) and ceramic composites [3],[4] via the reaction of metal cation with phosphate anions (**Fig. 2**). The reaction is attained by mixing a cation donor, generally an oxide (CaO [5],[6],[7],[8], MgO [2],[6],[9], ZnO [2],[8], Al_2O_3 [2], Fe_2O_3 [2],

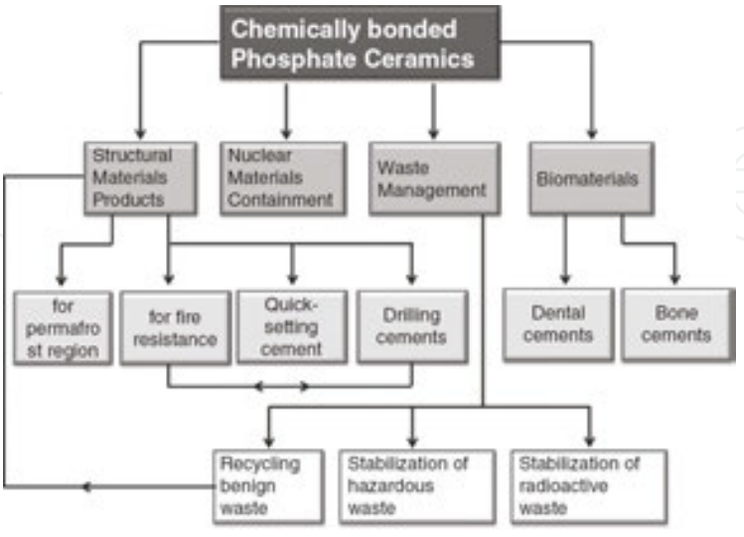

Fig. 2. Potential application of chemically bonded phosphate ceramics [1].

etc.), raw materials [10],or secondary raw materials (fly ash [11] and blast furnace slag [12]) with either phosphoric acid or acid phosphate such as ammonium phosphate solution or magnesium dihydrogen phosphate ($Mg(H_2PO_4)_2 \cdot 2H_2O$) and aluminum hydrogen phosphate ($AlH_3(PO_4)_2 \cdot H_2O$). Typical acid-base reaction between a metal oxide and phosphoric acid can be written as [2],[13]:

$$MO_x + n\ H_3PO_4 + m\ H_2O \rightarrow MH_{3n-2x}(PO_4)_n + (m+x)\ H_2O \quad (1)$$

where x denotes half of valence of **M**, $n \geq 2x/3$, and m is an arbitrary integer that decides the amount of water to be added in the reaction.

In the case of magnesium phosphate chemically bonded ceramics (MPCBC), the acido-basic **reaction 1** of orthophosporic acid with MgO yields the following products [2]:

$$MgO + 2\ H_3PO_4 \rightarrow Mg(H_2PO_4)_2 \cdot H_2O \quad \Rightarrow x = 1,\ n = 2,\ \text{and} m = 0 \quad (2)$$

$$MgO + H_3PO_4 + 2\ H_2O \rightarrow Mg(H_2PO_4)_2 \cdot 3H_2O \quad \Rightarrow x = 1,\ n = 1,\ \text{and} m = 2 \quad (3)$$

$$3\ MgO + 2\ H_3PO_4 \rightarrow Mg3(PO_4)_2 + 3\ H_2O \quad \Rightarrow x = 1,\ n = \frac{2}{3},\ \text{and} m = 0 \quad (4)$$

If acidic phosphate is used, the reaction proceeds as follows [2]:

$$MgO + Mg(H_2PO_4)_2 \rightarrow 2\ MgHPO_4 + H_2O \quad (5)$$

and similar reaction can be also written for the reaction of $Al(H_2PO_4)_3$ with $AlO_{3/2}$:

$$2\ AlO_{3/2} + Al(H_2PO_4)_3 \rightarrow 3\ AlPO_4 + 3\ H_2O \quad (6)$$

Reactions **5** and **6** indicate that partially acidic phosphate salt is only an intermediate phase. The dissociation of orthophosporic acid and the pH stability range of formed ionic species are given by **Eqs. 11–13** in **Chapter 9**. General dissociation reaction for acidic dihydrogen phosphate and its dissociation constant in the form of pK_{dis} ($pK_{dis} = -log\ K_{dis}$) can be written as follows:

$$M\left(H_2PO_4\right)_n \leftrightarrow M^{n+} + n\ \left(H_2PO_4\right)^{n-} \tag{7}$$

and

$$pK_{dis} = -\log\left(\left[M^{n+}\right]\left[H_2PO_4\right]^{n-}\right) \tag{8}$$

The values of pK_{dis} for KH_2PO_4, $(NH_4)H_2PO_4$, $Mg(H_2PO)_2{\cdot}2H_2O$ and $Ca(H_2PO_4)_2{\cdot}H_2O$ are 0.15, -0.69, 2.97 and 1.15, respectively [2].

The preparation scheme for the synthesis of aluminum phosphate binder is shown in **Fig. 3**. The evolution of chemical composition of phosphate binder with Al:P ratio of 1.4:3 with temperature is introduced by **Table 1**.

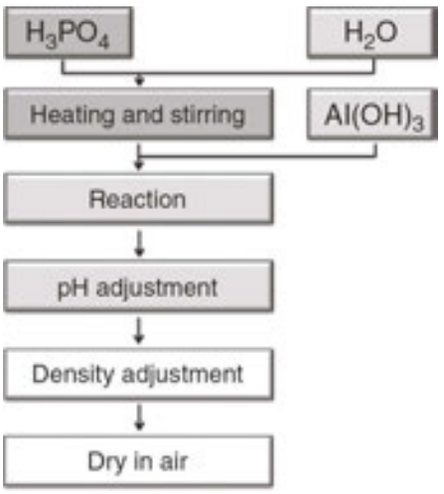

Fig. 3. Schematic procedure for the synthesis of aluminum phosphate binder [14].

Initially, the motivation for the development of these ceramic materials was the preparation of dental cements. Phosphate chemically bonded[1] ceramics (PCBC) find recently the application in diverse fields (**Fig. 2**), which include structural ceramics, refractory materials [15], toxic, radioactive [16],[17],[18],[19] or asbestos-containing[2] [20],[21],[22] waste management [23], oil drilling and bioceramics, pigments [1], etc. [2].

10.1.1. Ceramics and refractories

The broad term "ceramics" refers to any of a large family of materials that are usually inorganic and require high temperatures in their processing or manufacture. They are generally classified into glass, whitewares, including artware and structural ceramics, and refractories. In general,

[1] Chemical bonding as a means of solidification is very widely observed in nature. The formation of sedimentary rocks, such as carbonate rocks, lateritic soils and solidification of desert soils, are examples of this process [1].

Temperature [°C]	Dominant phase	Secondary phase
60	$AlH_3(PO_4)_2 \cdot 3H_2O$	—
105	$AlH_3(PO_4)_2 \cdot 3H_2O$ (monoclinic)	$Al(H_2PO_4)_3$ (hexagonal)
200	$Al(H_2PO_4)_3$ (hexagonal)	—
220	$AlPO_4$ (trigonal)	$AlH_2P_3O_{10} \cdot 2H_2O$
250		
300		
400	$Al(PO_3)_3$	$AlH_2P_3O_{10} \cdot 2.5H_2O$
500	$Al_2P_6O_{18}$	$Al(PO_3)_3$ (cubic)
600		
700		
800	$Al(PO_3)_3$ (cubic)	$AlPO_4$ (rhombic system)
900		
1000		

Table 1. The alteration of composition of phosphate binder with increasing temperature [14].

the term "glass" refers to an amorphous solid with non-directional properties, characterized by its transparency, hardness, rigidity at ordinary temperatures and capacity for plastic working at elevated temperatures. Major commercial uses of glass include plate or "float" glass, as used for windows and windshields; glass tubing, or formed shapes, used for electric lighting envelopes; and glass containers such as tumblers and bottles. Whiteware is characterized by a crystalline matrix held together by a glassy phase and usually covered by a glazed coating. Major classifications of whiteware are ceramic tiles, glazed and unglazed, for floors, walls and external use; sanitaryware in the form of toilets and lavatories; and tableware, from earthenware to fine china [24].

Kaolin is major raw material used for the fabrication of conventional ceramics. It is obtained from the alteration of granitoid rocks[3] [25]. It consists mostly of kaolinite and a small amount of impurities such as quartz, micas and other phyllosilicates. Firing of kaolinite induces numerous complex structural and microstructural transformations leading to the formation

[2] SEM picture of thin long fibrous structure of chrysotile ($H_4Mg_3Si_2O_9$ [20],[21],[22]) asbestos under the magnification of 98× (a), 5000× (b) and 10,000× (c).

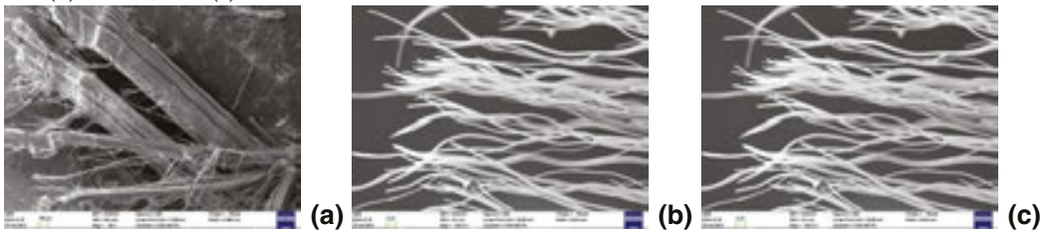

of mullite and silica (cristobalite) phase. Mullite phase is characterized by some advantageous properties such as good corrosion resistance, low dilatation coefficient, good creep and thermal shock resistances, thermal stability and high strength. These advantages make this phase favorable for different applications. Orthophosphoric acid reacts with aluminum from kaolin to provide new compounds, which are $Al(H_2PO_4)_3$ at room temperature and $AlPO_4$ when heated to temperatures above 800°C [10].

Approximately 70% of all refractories used in industry are in the form of bricks, which are cast in the shapes such as straights, soaps, splits, arches, wedges, keys, skews, jambs or other special and frequently patented shapes. Most industrial refractories are composed of metal oxides or of carbon, graphite or silicon carbide. Most refractory bricks are shaped by combining the size-graded refractory aggregate with a small amount of moisture and casting in a dry press. The important properties of any refractory, including its high-temperature strength, depend on its mineral makeup, the particle-size distribution of minerals and the way these materials react at high temperatures and in furnace environments. When a refractory is chosen for a particular service, the service conditions must be considered in the design. In proper selection of a refractory, these factors, together with an economic balance, must be considered so that the refractory ultimately produces the lowest cost per unit weight of product per unit weight of refractory consumed [26].

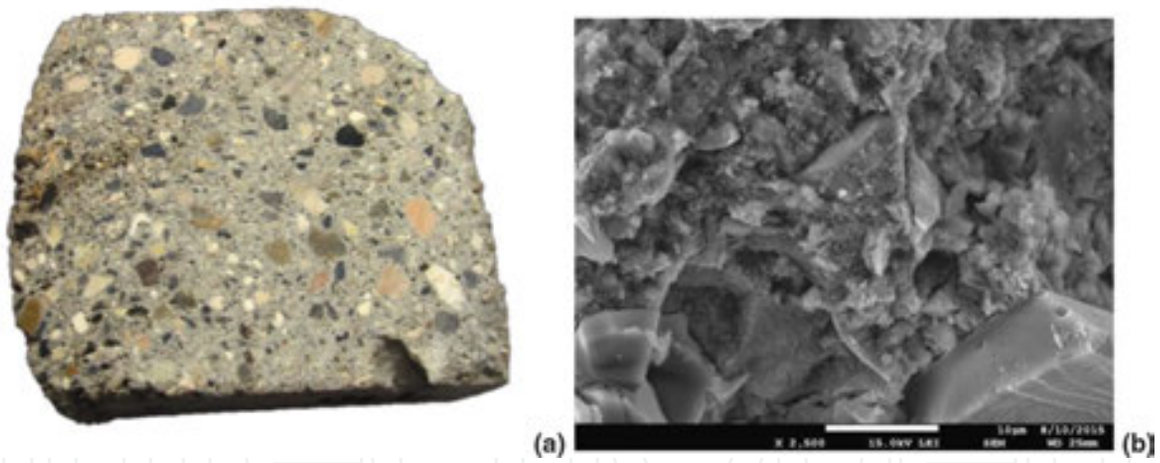

Fig. 4. Cutting plane throughout the block of chemically phosphate bonded refractory material containing large grains of calcined bauxite (a) and electron microscopy (SEM) picture of ceramic body (b).

The materials must be chosen with generous safety margins in the temperature capability and the refractory construction system, whether brick, monolithic or fiber, should be suitable not only for the operating conditions but also for the type of equipment concerned and the construction conditions. Refractory concretes and castables (monolithic refractories) are especially suitable for these small burner quarls. Fibers and refractory ceramic fibers (glass,

[3] Granular crystalline rock consisting essentially from quartz, orthoclase-feldspar and mica. Usually is light gray, white or light in color [25].

mineral, ceramic fibers and whiskers) become an important construction as well as insulation material, although the brickwork has the longest history of the development [27].

Aluminosilicate refractories are manufactured using refractory clays, sillimanite minerals, bauxite (**Fig. 4**) and mixtures of alumina and silica sand. They will refer, somewhat arbitrarily, to common crystalline compounds with melting temperatures of at least 1500°C. The major categories of traditional refractories are fire clays, high alumina and silica. The choice of material for traditional refractory applications, as well as for advanced material applications, was and is based on balancing the cost and the performance lifetime [28].

Industries involved in steel melting and casting of special alloys are always interested in using the maintenance-free, functional refractories to achieve energy-efficient metal processing. They seek for the development of new and advanced thermal ceramics for protective thermal insulation linings and molten metal handling crucibles. Conventionally, porous to dense Al_2O_3, SiO_2, MgO, ZrO_2, SiC[4] [29] and fireclay ceramic bodies were used as thermal insulation refractory liners [30]. Phosphate bond can also be utilized in manufacturing of refractory and wear-resistant and of protective coatings on metal [14] or ceramic surfaces [31]. Intensive development of ceramic materials has increased the availability of well-characterized engineering ceramics capable of the utilization over the range of temperatures and atmospheres [32].

Refractory castables can be classified according to different aspects including the content of calcium, binder source, overall chemical composition, bulk density, application method and others. Binders commonly used in monolithic products may be of various classes [33]:

1. Hydraulic (cement and hydratable alumina) [34]
2. Chemical (phosphoric acid, silicates, geopolymers, etc.) [33],[35]
3. Sol-gel (colloidal silica or alumina) [33]

Regarding the chemical ones, the bond strength can be provided by the addition of phosphates (dry or solution) or by in situ generation of phosphates (formed via the reaction with added H_3PO_4) in the refractory structure. The reaction of Al_2O_3 or $Al(OH)_3$ with orthophosphoric acid can be described by reactions [33]:

$$6\ H_3PO_4 + Al_2O_3 \rightarrow 2\ Al\left(H_2PO_4\right)_3 + 3\ H_2O \tag{9}$$

$$3\ H_3PO_4 + Al\left(OH\right)_3 \rightarrow Al\left(H_2PO_4\right)_3 + 3\ H_2O \tag{10}$$

A cold-setting refractory material was developed by Hipedinger et al [36] via the magnesia-phosphate reaction. A cement paste based on alumina, silica fume, magnesia and orthophosphoric acid or monoaluminum phosphate was designed to form cordierite-mullite during

[4] It was proved that H_3PO_4 is effective binder for SiC [29].

heating. This cement paste set at room temperature and $MgHPO_4 \cdot 3H_2O$ phase (newberyite) was observed, but amorphous phases were predominant. Two exothermic effects were detected during the setting process corresponding to the acido-basic reaction of magnesia with phosphates and to the formation of bonding hydrates. At 1100°C, *c*-$AlPO_4$ was formed by the reaction of alumina with orthophosphoric acid or monoaluminum phosphate. At 1350°C, the dominant crystalline phases were cordierite and mullite. A refractory concrete with obtained cement paste and a cordierite-mullite aggregate (scrap refractory material) was prepared.

The acid phosphate impregnation, with ozone pretreatment, improves the oxidation resistance of carbon materials (polycrystalline graphite and pitch-based carbon fiber), as shown by the weight measurement in air up to 1500°C. The impregnation involves using phosphoric acid and dissolved aluminum hydroxide in the molar ratio of 12:1 and results in rough, white and hard aluminum metaphosphate coating of the weight of about 20% of that of the carbon before the treatment. Without ozone pretreatment, the impregnation is not effective. Without aluminum hydroxide, the impregnation even degrades the oxidation resistance of carbon [37].

10.1.2. Dental phosphate cement

A variety of cements are used in modern clinical dentistry, such as glass ionomers, zinc phosphate and zinc polycarboxylate [38],[39]. Dental zinc phosphate cement is primarily used for the cementation of indirect restorations, such as crown and bridges. It has the longest record of any cement, approximate 100 years, and has remained popular throughout this time. Zinc phosphate cements are also considered the strongest among the dental cements. However, it is also applied for temporary fillings, cavity bases and buildings of teeth beneath crowns. Zinc phosphate cement is primarily in contact with the pulp-dentin system and in certain cases (e.g. temporary fillings) with the gingiva. A variety of cementing materials are currently used as the bases and luting[5] agents, but zinc phosphate cement has been used for many decades. Phosphoric acid-based cements originated from Ostermann´s formula from 1832, which was composed of calcium oxide and anhydrous phosphoric acid. In 1902, Fleck established a formula that is similar to that being in use today [40],[41],[42],[43],[44].

The powder is mainly a mixture of zinc oxide and up to 13% magnesium oxide. The liquid is an aqueous solution of phosphoric acid containing 38 – 59% H_3PO_4, 30 – 55% water and 0 – 10% zinc. Aluminum is essential to the cement-forming reaction, and zinc moderates the reaction between powder and liquid, allowing adequate working time and sufficient quantity of powder to be added for optimum properties of cement. When the powder is mixed with liquid, phosphoric acid attacks the surface of particles, dissolving zinc oxide, which releases zinc ions into the solution. Aluminum in the liquid reacts with phosphoric acid to form zinc aluminophosphate gel on remaining portion of particles. Thus, the cement reveals a cored structure consisting primarily of non-reacted zinc oxide particle core embedded in a cohesive amorphous matrix of zinc aluminophosphate (glasslike phosphate). Aluminum phos-

[5] The word 'luting' implies the use of a molded or moldable article to seal a space or to cement two components together [44].

phate, in addition to its role as a retarder, contributes to the increase in mechanical hardness of cement [40],[45].

Setting reactions and resultant structure of zinc phosphate cements are largely based on the formation of hopeite ($Zn_3(PO_4)_2{\cdot}4H_2O$) and/or zinc phosphate hydrate ($Zn_2P_2O_7{\cdot}3H_2O$) when using orthophosphoric acid (OPA) cement-forming liquids. OPA solutions buffered with aluminum and zinc ion produced better mechanical properties than non-buffered OPA solutions because of the formation of hopeite and amorphous phase. The development of crystalline forms of phosphate hydrates of zinc and magnesium was retarded and/or prevented by the incorporation of aluminum and zinc ion in the cement-forming liquid [43].

This mechanism is similar to the cement-forming reaction described by Wilson [43],[46] in a dental silicate cement (**Fig. 5**). When H^+ ions attack the glass powder, Al^{3+}, Ca^{2+}, Na^+ and F^- are liberated from the glass, leaving behind an ion-depleted layer of silicate gel at the surface of glass particles. Liberated ions migrate and react with $H_2PO_4^-$, and salts precipitate. The principal reaction is the formation of an insoluble aluminum phosphate, the gel matrix. Associated side reactions are the precipitation of calcium fluoride and the formation of soluble sodium dihydrogen phosphate.

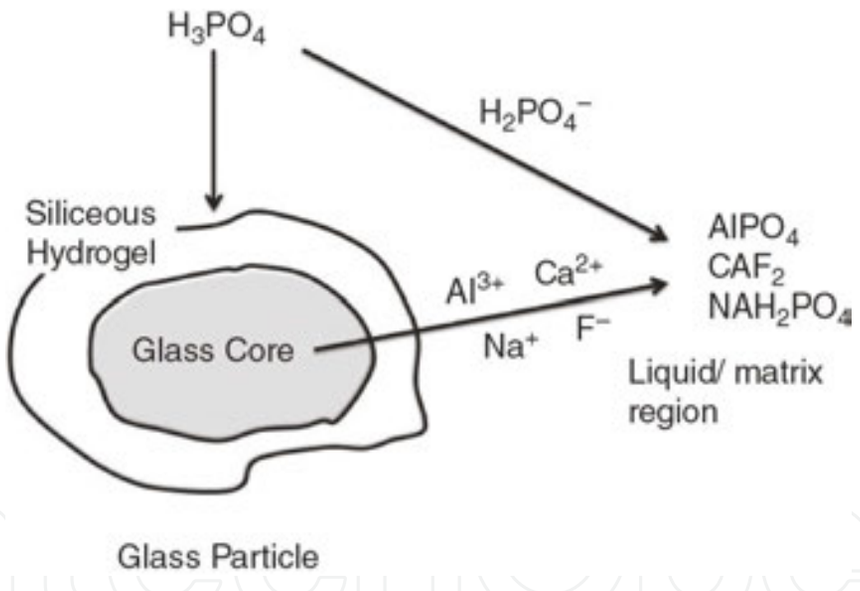

Fig. 5. Setting reaction of dental silicate cement [43].

10.2. Oil-well cement

The main application of the cement in an oil well is to stabilize the steel casing in the borehole and to protect it from corrosion. The cement is pumped through the borehole and is pushed upwards through the annulus between the casing and the formation. The cement is exposed to the temperature and pressure gradients of the borehole [47].

Various types of oil-well cements are distinguished. The most important is the phase composition of cement, primarily the C_3A phase content, which causes quick paste thickening. The main feature of oil-well cement is that it must remain sufficiently fluid for a long period, required for its pumping to deep well. Simultaneously, the temperature in the borehole increases with depth[6] [48],[49]. The types and properties of oil-well cements specified by the American Petroleum Institute (API) are introduced by Clinkers containing limestone loess, diatomite, pyritic ash and sand modified with gypsum and apatite were used for the manufacture of heat resistant oil-well cements. Apatite is also a good stabilizer for high belite cements [50].

API class	Special properties	Intended use
A	Same as ASTM Type I	Well depths up to 1800 m and temperatures of 27 – 77°C.
B	Similar to ASTM Type II, low C_3A, high sulfate resistance	
C	Similar to ASTM Type III, low C_3A, high sulfate resistance	Well depths up to 1800 m and temperatures of 80 – 170°C.
D	Low C_3A with set retarder	Depths up to 1800 – 3600 m and temperatures of 77 – 138°C.
E		Depths up to 1800 – 4200 m and temperatures of 77 – 138°C.
F		Depths up to 3000 – 4800 m and temperatures of 127 – 160°C.
G and H	Coarse-ground ASTM Types II and IV	Temperatures of 27 – 93°C.
J	Essentially β-C_2S and pulverized silica sand	Depths below 6000 m and temperatures > 177°C

Table 2 Types and properties of oil-well cements [49].

10.3. Phosphate glasses and glass-ceramics

In the past decades, optical waveguides have raised great interest, as they are the most fundamental and integral part of integrated optic circuits. Glass-based integrated optical devices have several obvious advantages over other technologies such as low intrinsic absorption in near-infrared region of the spectrum, minimized coupling losses to optical fibers and no intrinsic material birefringence compared to crystalline semiconductors. Phosphate glasses are regarded as excellent glass host for the waveguide laser fabrication mainly because of high solubility of rare-earth ions compared to other oxide glasses, which allows for high doping concentrations without significant lifetime reduction, resulting in high gain in short waveguides or cavities and a desirable feature in single-frequency lasers. High-performance

[6] The rate depends on the geothermal degree, which in Europe is about 33 m·°C^{-1} [48].

waveguide amplifiers or lasers are fabricated in various earth-ion-doped phosphate glasses and commercial phosphate glasses such as Kigre Q89 and Schott-IOG 1 [51].

Glass-ceramics are polycrystalline materials with an inorganic–inorganic microstructure, which are prepared from the base glass by controlled crystallization. This can be achieved by subjecting glasses to regulated heat treatment, which results in the nucleation and growth of one or more crystal phases within the glass [52]. Once a stable crystal nucleus has formed and begun to grow, there are a number of possible crystal growth mechanisms and these determine the final crystal morphology [53],[54]:

a. **Faceted crystal growth**: the favored growth sites on an atomic scale are the steps in rows of atoms. However, these sites can be easily eliminated by the very growth that they promote. Despite this, several types of lattice or crystal defects were shown to provide the growth sites that are impossible to be eliminated by the growth.

b. **Dendritic crystal growth**: formed dendritic crystals are characterized by their tree-like appearance. This type of solidification usually takes place in metals and sometimes occurs naturally in silicate minerals, especially in olivine during rapid cooling of lavas.

c. **Spherulitic crystal growth**: is most commonly associated with organic polymeric materials. The geological definition of a spherulite is: "A crystalline spherical body built of exceedingly thin fibers radiating outwards from a center and terminating on the surface of the sphere…".

Bioactive glass-ceramics are an alternative to synthetic HAP (**Section 10.9**) for the use in vivo both in restorative dental applications and in bone implantation [54],[55]. Artificial materials implanted into the bone defects are generally encapsulated by fibrous tissue isolating them from the surrounding bone. This is the normal response of the body towards inert artificial materials. However, some ceramics, such as bioglass, A-W glass-ceramics and sintered hydroxyapatite form a bone-like apatite on their surfaces in the living body and bond to living bone through this apatite layer. This bone-bonding ability is called the bioactivity [56].

These bioactive ceramics are already used clinically as important bone-repairing materials. Their bone-bonding ability is achieved by the formation of a biologically active apatite layer after the reaction of the ceramics with surrounding body fluid. Controlled surface reaction of the ceramics is an important factor governing its bioactivity as well as its biodegradability [56]. The preparation of glass-ceramics with high CaO/P_2O_5 ratio, containing large amounts of calcium phosphate crystals, is believed to be one of the best approaches to obtain the bioceramic implants suitable for bone replacement/regeneration [57].

10.3.1. Alkaline aluminum phosphate glasses

Alkaline aluminum phosphate glasses (NMAP) with excellent chemical durability for thermal ion-exchanged optical waveguide were investigated by Wang et al [51]. The transition temperature (T_g = 470°C) is higher than the ion-exchange temperature (390°C), which is favorable for sustaining the stability of the glass structure for planar waveguide fabrication. The glass-forming region in the Na_2O-Al_2O_3-P_2O_5 system is shown in **Fig. 6** [51],[58].

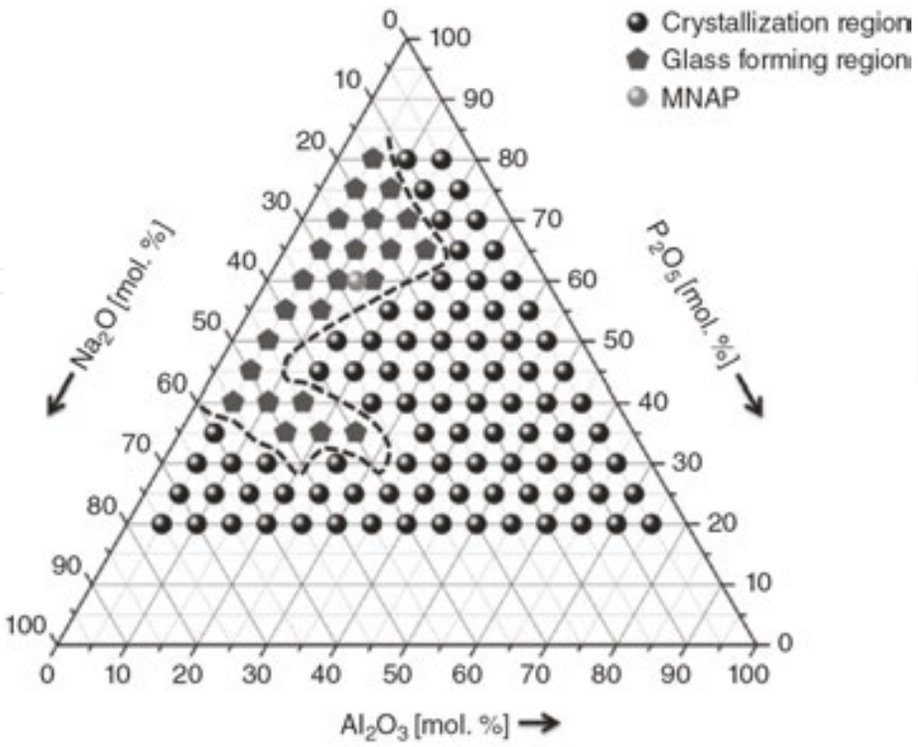

Fig. 6. Ternary phase diagram of Na_2O-Al_2O_3-P_2O_5 system [51],[58].

10.3.2. Iron phosphate glasses

Iron phosphate glass is a versatile matrix for the immobilization of various radioactive elements found in high-level nuclear waste (HLW). Among various compositions of iron phosphate glass, the one with 40 mol.% Fe_2O_3-60 mol.% P_2O_5 was found to be chemically durable. It also has the ability to accommodate large amounts of certain nuclear wastes, especially those that are not well suited for borosilicate glasses. Better chemical durability of iron phosphate glass is attributed to the presence of more hydration-resistant Fe-O-P bonds compared to P-O-P bonds available in other phosphate glasses [59],[60],[61].

10.3.3. Lithium vanado-phosphate glasses

Lithium vanado-phosphate (LiVP) glasses have been largely studied due to their potential application as cathode materials as a result of mixed electronic-ionic conductivity character.[7] Furthermore, lithium and vanadium structural rearrangements in the glass matrix could modify the transport properties of the systems. Interestingly, the modifier ions depolymerize the glass network, creating useful channels that enhance the ionic conductivity, but they can also break some V^{4+}/O/V^{5+} linkages that are essential to the electronic conductivity because they are supposed to be the preferential path for small polaron hopping. The population of

[7] Fast ion conducting (FIC) phosphate glasses have become very important due to a wide range of applications in solid-state devices [63].

$V^{4+}/O/V^{5+}$ paths depends even on the V/P ratio and it can modify the main structure role of vanadium ions in glasses [62],[63],[64].

10.3.4. Apatite-wollastonite glass-ceramics

Wollastonite ($CaSiO_3$) is white glassy silicate mineral that occurs as masses or tabular crystals of metamorphosed limestone. A silica chain GC that contained crystalline apatite and wollastonite (AW) was introduced in MgO-CaO-SiO_2-P_2O_5 glassy matrix and it showed excellent bioactivity, biocompatibility, machinability and adequate mechanical properties such as Young's modulus (117 GPa), compressive strength (1080 MPa) and bending strength (215 MPa) [52],[65],[66],[67].

Wollastonite-2M and pseudowollastonite (low- and high-temperature forms of wollastonite, respectively) are the most common calcium silicate biomaterials proposed for bone tissue regeneration [68]. The major drawback of the $CaSiO_3$ bioceramics is their relatively fast dissolution rate that could reduce their mechanical strength. In addition, the pH of surrounding medium significantly increases, which could affect the osseointegration of the substitute material within the natural bone. The problem can potentially be solved by the development of multiphase materials containing highly dissolvable phases such as wollastonite, on one hand, and stable phases such as HAP, on the other hand [69].

From the bioactive ceramics, the A/W glass-ceramics show high bioactivity and high mechanical strength [56]. The A/W glass-ceramics composed of apatite and wollastonite crystalline phases in a glassy matrix was developed by Kokubo [70]. This bioceramics is highly bioactive and also mechanically strong in comparison with other glasses and glass-ceramics because of wollastonite and apatite crystals' presence.

The A/W glass-ceramics is used in some medical applications, either in powder form as a bone filler or as a bulk material. These materials are currently manufactured by the powder processing methods, providing uniform crystallization of apatite and wollastonite phases in the glassy matrix, as the crystallization of parent glass in a bulk form leads to the appearance of large cracks [69],[71]. The glass-ceramics exposed to the SBF releases predominantly Ca and Si ions, due to the dissolution of amorphous phases and wollastonite-2M, leading to the formation of an apatite-like layer on the surface of the material [69].

The addition of ZnO increased the chemical durability of A-W glass-ceramics, resulting in a decrease in the rate of apatite formation in simulated body fluid. On the other hand, the release of zinc from the glass-ceramics increased with increasing ZnO content. The addition of ZnO may provide bioactive CaO-SiO_2-P_2O_5-CaF_2 glass-ceramics with the capacity for appropriate biodegradation as well as the enhancement of bone formation [56]. The effect of MgO was investigated by Ma et al [72]. As the MgO content increased, the glass crystallization temperature increased and the crystallization of the glass-ceramics was changed from the bulk crystallization to the surface crystallization. The addition of MgO slowed down the rate of dissolution and retarded the formation of apatite layer.

10.3.5. Apatite-mullite glass-ceramics

Apatite-mullite glass-ceramics crystallize from the glass of generic composition SiO_2-Al_2O_3-P_2O_5-CaO-CaF_2 to form an osseoconductive apatite phase existing as spherulites within a mullite matrix. The formation of apatite spherulites is accompanied by a depletion zone, from which calcium, phosphate and fluorine is taken and added to the growing crystal. The depletion zone also inhibits the formation of further apatite crystals in the immediate vicinity due to the glass' compositional similarity with a mullite composition. As mullite begins to crystallize, there is interdependence between the growth of apatite and mullite. Spherulitic grain boundaries in partially devitrified apatite-mullite ceramics act as crack promoters, offering preferential paths to propagation due to the grain boundary interfacial surface energy [54],[73].

10.3.6. FAP-anorthite-diopside glass-ceramics

There is a considerable interest in oxyfluoride glasses and glass-ceramics for laser amplifiers and up-conversion processors. Fluoride-containing crystals have low phonon energies and apatite crystals, in particular, are good host phases to adsorb rare-earth ions. Fluoride-containing glass-ceramics also often crystallize on a nanoscale, which is an added advantage, since optically transparent materials are required for the applications such as fiber amplifiers. The evidence of the nanoscale crystallization in an FAP-anorthite-diopside-based glass-ceramics was found by Hill et al [74].

10.3.7. Apatite-wollastonite ceramics

Wollastonite-hydroxyapatite ceramics was successfully prepared by a novel method, corresponding to the thermal treatment of a silicone embedding micro- and nanosized fillers in air. $CaCO_3$ nanosized particles, providing CaO upon the decomposition, acted as "active" filler, whereas different commercially available or synthesized hydroxyapatite particles were used as "passive" filler. The homogeneous distribution of CaO, at a quasi-molecular level, favored the reaction with silica derived from the polymer, at only 900°C, preventing extensive decomposition of hydroxyapatite. Open-celled porous ceramics suitable for scaffolds for bone-tissue engineering applications were easily prepared from the filler-containing silicone resin mixed with sacrificial PMMA microbeads as the templates [75].

10.3.8. Oxyapatite glass-ceramics

The crystallization of oxyapatite of the composition $NaY_9(SiO_4)_6O_2$ ($P6_3/M$, $\boldsymbol{a}$ = 9.334 Å and $\boldsymbol{c}$ = 6.759 Å, c:a = 1:0.7241, V = 509.97 Å, **Fig. 7**) from three different glasses from the SiO_2-B_2O_3-Al_2O_3-Y_2O_3-CaO-Na_2O-K_2O-F glass-ceramics system with different F and B_2O_3 content after the

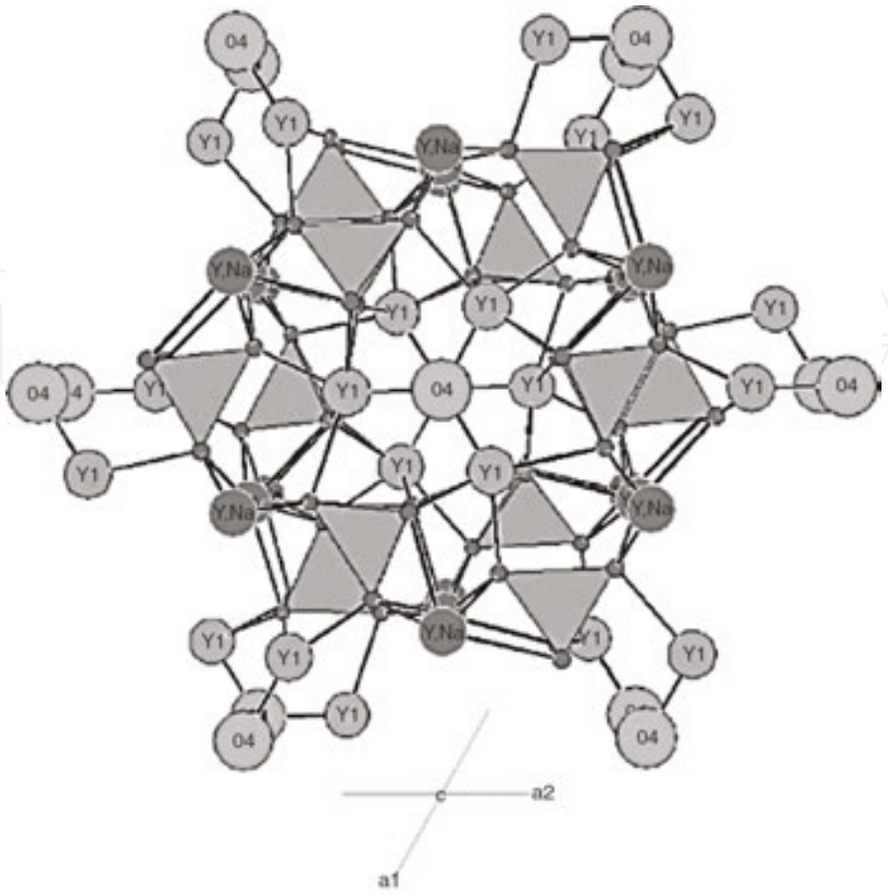

Fig. 7. Crystal structure of oxyapatite $NaY_9(SiO_4)_6O_2$ (perspective view along the *c*-axis) where the tetrahedra represents $[SiO_4]^{4-}$ structural units [76].

heat treatment was observed by VAN´T HOEN et al [76]. The formation of oxyapatite proceeds according to the mechanism of controlled surface nucleation and crystallization. Therefore, applying suitable chemical composition and heat treatment, it is possible to produce glass-ceramics containing oxyapatite crystals. This type of crystal exhibits similar crystal structure as that of fluorapatite. Therefore, there is an isotype relationship between those two phases: the differences in the crystal structures are found in the structural units, with fluorapatite containing $[PO_4]^{3-}$ and $[F]^{-}$, while oxyapatite containing $[SiO_4]^{4-}$ and $[O]^{2-}$. Because of its specific optical properties (high opacity), this new glass-ceramic material may be used as layering material for dental restoration [76].

10.4. Solid oxide fuel cells

Solid oxide fuel cell (SOFC) is an electrochemical energy-conversion device, which offers tremendous promise for delivering high electrical efficiency and significant environmental benefits in the terms of fuel flexibility (hydrocarbons and municipal waste) as well as clean and efficient (>70% with fuel regeneration) electric power generation. SOFC produces useful

electricity by the reaction of fuel with an oxidant via the diffusion of oxide ions (or protons) through an ion-conducting solid-electrolyte layer [77].

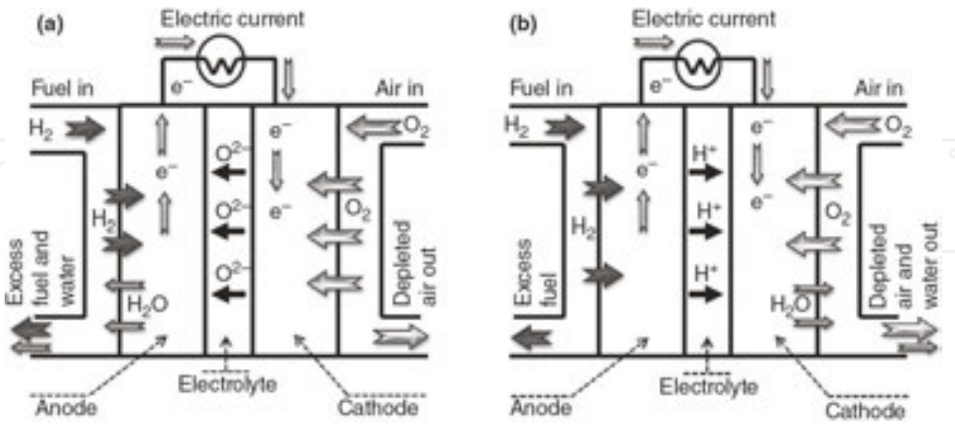

Fig. 8. Schematic diagram of solid oxide fuel cell (SOFC) showing non-ion-conducting electrolyte (a) and proton-conducting electrolyte during its operation (b) [77].

SOFC is composed of a dense electrolyte layer that is sandwiched between two porous electrodes (i.e. cathode and anode) as shown in **Fig. 8**. SOFC can use either oxide ion (a) and/or proton conduction through the electrolyte (b). Electrons generated through the oxidation of fuel on anode are accepted for the oxygen reduction on cathode, which completes the external circuit. The electricity is, thus, produced by the flow of electrons in the external circuit (from the anode to the cathode). Since the current is obtained via the diffusion of oxide ions (or protons) through a solid electrolyte, it becomes imperative to use high operating temperatures (~800 – 1000°C) for achieving high ionic conductivity (of ~0.1 $S \cdot cm^{-1}$) [77],[78].

The first fuel cell was invented in 1838 by an English scientist, William Grove. He named it "wet cell battery" or "Grove cell", which operated by reversing the electrolysis phenomena of water [77],[79]. The fuel cell, invented in 1839 by Grove, is an electrochemical device that converts the chemical energy of fuels directly into electricity and heat by electrochemically combining H_2, CO/H_2 or reformed hydrocarbons in fuel and an oxidant gas transported via an ion-conducting electrolyte. Direct combustion of fuels is eliminated here, which renders the fuel cells much higher conversion efficiencies compared to other conventional thermomechanical methods. Moreover, with fuel cells, the power generation is virtually noise-free and can produce 0.9 times lower emissions of NO_x and SO_x per unit of power output compared to that of conventional technologies. Additionally, it is possible to use the fuel cells for combined heat and power (CHP or cogeneration) generation [77],[80].

The development of high-performance SOFC involves the material selection and operation-related issues (of anode, cathode, electrolyte, sealant and interconnects). These challenges open up the myriad research opportunities for researchers in the field of SOFC. A list of various materials used in SOFC is presented in **Fig. 9**.

http://dx.doi.org/10.5772/62217

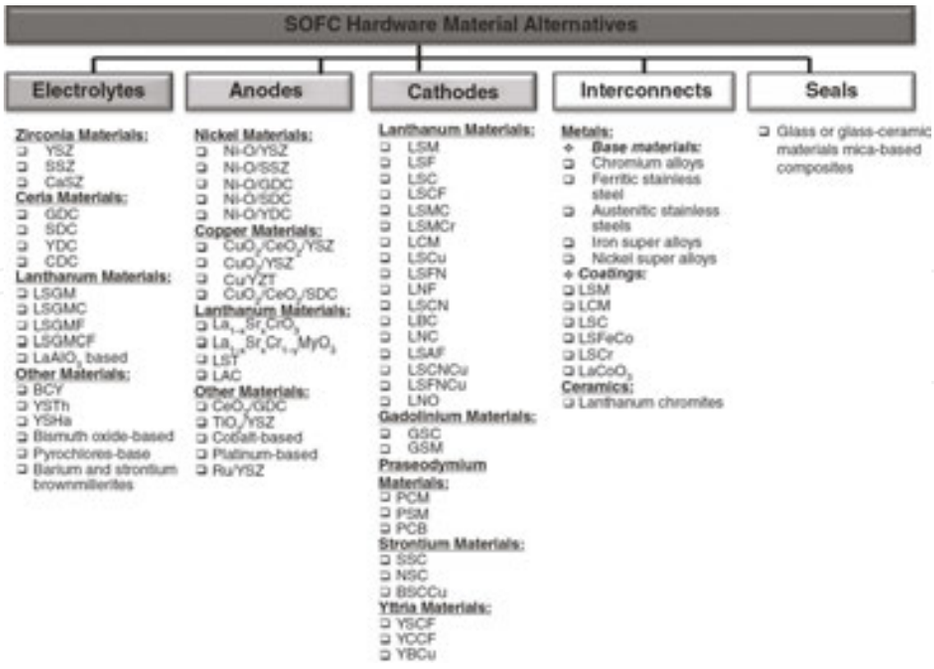

Fig. 9. Comprehensive list of various materials used in SOFC [77].

Apatite-type silicates are considered as promising electrolytes for solid oxide fuel cells. Lanthanum silicate with the composition of $La_{10}Si_{5.5}Al_{0.5}O_{26.75}$ was evaluated as an electrolyte with the electrode materials commonly used in SOFC, i.e. manganite, ferrite and cobaltite as cathode materials and NiO-CGO composite, chromium-manganite and Sr_2MgMoO_6 as anode materials by Marrero-López et al [81]. This electrolyte has conductivity values higher than those of YSZ and comparable to most important solid electrolytes proposed for the intermediate-temperature range, such as doped ceria and lanthanum gallate-based electrolytes. The chemical compatibility did not reveal appreciable bulk reactivity between silicate and many electrodes up to 1300°C [81]. Among several reported rare earth apatites, lanthanum silicates exhibit the ionic conductivity higher than their germinate counterparts [77].

On examining and modeling the probable conduction mechanism in apatite silicates, the atomistic simulation results suggest that the conduction in $La_{9.33}(SiO_4)_6O_2$ and $La_8Sr_2(SiO_4)_6O_2$ takes place via interstitial and vacancy mechanism, respectively [82],[83]. The predicted pathway appears to be a complex nonlinear "sinusoidal-like" process for the interstitial oxygen migration along the c-axis (**Fig. 10**), while a direct linear pathway is predicted for oxygen migration via the vacancy mechanism [77].

Zeng et al [84] developed a model capable of prediction of oxygen ion conduction from relative Coulomb electronic interactions in oxyapatites and rationalized observed experimental trends reported in the literature. Two types of fundamental chemical property, i.e. the electronegativities and ionic radii of the constituents, control oxygen ionic conduction in oxyapatites. Those two properties were used to represent the relative charge densities and the distances between charged units, respectively, and then to formulate the relative Coulomb energy. It was found that this relative Coulomb energy is linearly correlated to the oxygen ionic

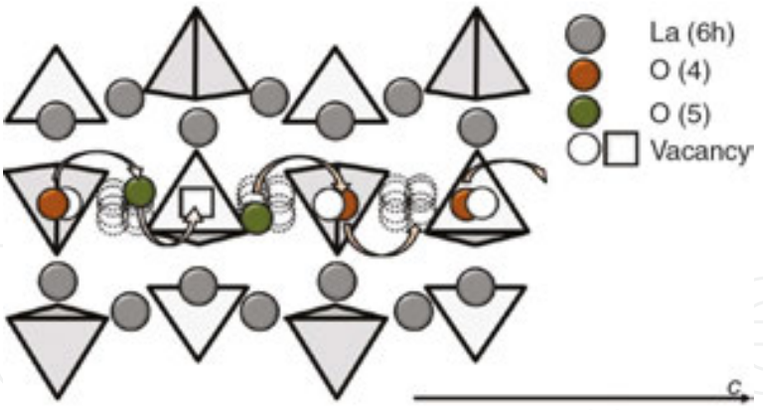

Fig. 10. Structural defect position and possible conduction mechanism along the c-axis representation of two adjacent unit-cells [77].

conductivity (in logarithmic form) in the oxyapatite systems. Doping a cation with large ionic radius and low electronegativity tends to increase the ionic conductivity of oxyapatite.

The c-axis-oriented apatite-type lanthanum silicate ($La_{10}Si_6O_{27}$) ceramics was prepared by NAKAYAMA et al [85] via the sintering process under high magnetic field. The degree of orientation in the $La_{10}Si_6O_{27}$ ceramics sintered at 1700°C was 48.1%. The conductivity of the c-axis-oriented ceramics is about 0.5 orders of magnitude higher than that of non-oriented ceramics. Higher conductivity is caused by the orientation of oxide ions in the grains composing the ceramics, which are located along the c-axis and are responsible for the ionic conduction.

10.5. Sensors

Compacted sinters of $Ln_{9.33+x/3}Si_{6-x}Al_xO_{26}$ ($0 \leq \boldsymbol{x} \leq 2.0$, Ln = La, Nd and Sm) are composed of an apatite-like phase with a hexagonal structure. Compacted sinters were used as potentiometric oxygen sensors (**Fig. 11**). The concentration dependence of EMF was well expressed by the Nernst equation:

$$E_{obs} = \frac{RT}{nF} \ln \frac{p_{O_2}(I)}{p_{O_2}(II)} \tag{11}$$

Furthermore, the electron number ***n*** is comparable to the theoretical value of 4. The sensing characteristics of the sinters are comparable to those of the sensors with 3 and 8 mol.% YSZ [86].

http://dx.doi.org/10.5772/62217

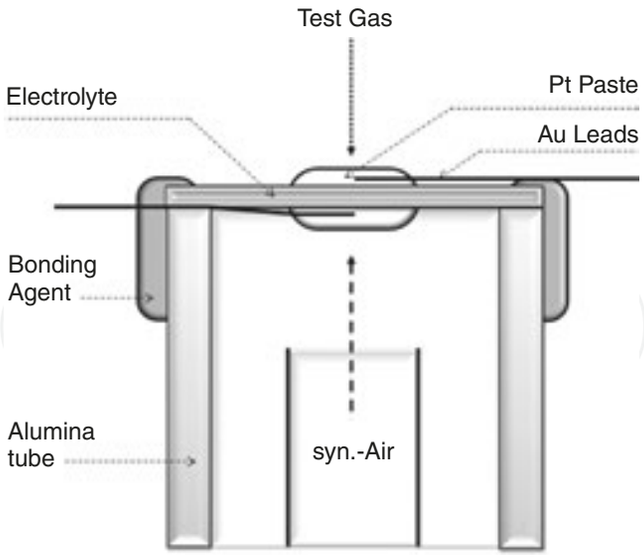

Fig. 11. Schematic picture of the O_2 concentration cell with the electrolyte of $Ln_{9.83}Si_{4.5}Al_{1.5}O_{26}$ where Ln = La, Nd and Sm [86].

Electrical properties and humidity sensor characteristics of lead hydroxyapatite material were reported by TUDORACHE et al [87]. The electrical characteristics of lead hydroxyapatite material treated at different temperatures made us focus on the analysis of the influence of water vapors upon the electrical characteristics. Thus, the electrical response to humidity adsorptive processes of lead hydroxyapatite material suggested that we analyze the material characteristics in terms of its use as a humidity sensor.

The humidity-sensitivity of yttrium-substituted calcium oxyhydroxyapatites was studied by OWADA et al [88]. The logarithm of electrical resistance of the present sensors decreased linearly with increasing relative humidity (RH) from 30 to 65%. The resistance of $[Ca_{9.0}Y_{1.0}](PO_4)_6[O_{1.5}\square_{0.5}]$ with the highest OH vacancy content was about one order of magnitude lower than that of calcium hydroxyapatite. It was found that the larger ratio of surface hydroxyl groups per unit surface area in the sample, the lower the resistance and the higher the amount of OH vacancies.

Using the hydroxylapatite ceramics as CO_2 sensor, which is based on electrical conductivity changes, was investigated by NAGAI et al [89]. Starting powders prepared by usual wet process were cast in film with an organic vehicle and fired on alumina substrates after the electrodes had been arranged. It was necessary to soak the samples in a $CaCl_2$ solution in order to make them reactive with CO_2. Both D.C. and A.C. measurements were carried out in various atmospheres including air, CO_2 and air containing different amounts of CO_2.

10.6. Phosphors

Fluorescent lamps typically have transparent glass envelope enclosing sealed discharge space containing an inert gas and mercury vapor. When subjected to a current provided by electro-

des, mercury ionizes to produce the radiation having the primary wavelengths of 185 nm and 254 nm. This ultraviolet radiation, in turn, excites phosphors on the inside surface of the envelope to produce visible light that is emitted through the glass. Generally, the fluorescent lamp for illumination uses a phosphor that absorbs the 254 nm Hg-resonance wave; the phosphor is activated so as to convert the ultraviolet light into the visible light. In order to improve the color-rendering properties and the emission output of fluorescent lamps, efficient illumination of a white color has been recently provided using a three-band-type fluorescent lamp, which employs a mixture of red, green and blue-emitting phosphors. In such three-band-type phosphor lamp, the emitting colors of the respective phosphors are considerably different from one another. Therefore, if the emitting intensity of any of the three corresponding phosphors is decreased, the color deviation occurs, degrading the color-rendering properties of the lamp [90]. The literature dedicated to the preparation of apatite-type light-emitting phosphors is really abundant.

A series of orange-red-emitting $Ba_2Y_3(SiO_4)_3F:xSm^{3+}$ ($0.003 \leq \boldsymbol{x} \leq 0.08$) fluorosilicate apatite phosphors were synthesized via the conventional solid-state reaction by Yu et al [91]. The emission spectra of the $Ba_2Y_3(SiO_4)_3F:Sm^{3+}$ phosphors contained some sharp emission peaks of Sm^{3+} ions centered at 564, 601, 648 and 710 nm. The strongest one is located at 601 nm. The optimum dopant concentration of Sm^{3+} ions in $Ba_2Y_3(SiO_4)_3F:xSm^{3+}$ is around 3 mol.% and the critical transfer distance of Sm^{3+} was calculated to be 26 Å. The quenching temperature is above 500 K.

Red-emitting phosphors $Ba_2Gd_8(SiO_4)_6O_2:Eu^{3+}$ ($BGS:Eu^{3+}$) with silicate apatite structure were prepared by Liu et al [92] via the conventional high-temperature solid-state reaction method. There are two different sites (4*f* and 6*h* [93]) for Eu^{3+} occupying the host. It was found that the phosphors $BGS:Eu^{3+}$ exhibit red emission with high quenching concentration at ~70.75 at.%, and the critical transfer distance of Eu^{3+} in $BGS:Eu^{3+}$ was calculated to be ~12.3 Å. More importantly, it has better CIE chromaticity coordinate for white light-emitting diode (w-LED) application in comparison with commercial phosphor $(Y,Gd)BO_3:Eu^{3+}$ ($YGB:Eu^{3+}$) under near-ultraviolet (n-UV) 393 nm excitation [92],[94]. White Tb^{3+}/Sm^{3+} ions co-doped $Ca_2La_8(GeO4)_6O_2$ (CLGO) phosphors prepared by Jeon et al [95] show observable emission spectra under 374 nm excitation.

A novel blue-emitting phosphor $Sr_8La_2(PO_4)_6O_2:Eu^{2+}$ was synthesized by Liu et al [96] via conventional high-temperature solid-state method and its photoluminescence (PL) properties were investigated for the applications in white light-emitting diodes. The phosphor exhibited strong broad absorption band in the near-ultraviolet (n-UV) range and generated bright-blue emission centered at 442 nm upon 365 nm excitation light. The critical Eu^{2+} quenching concentration (QC) mechanism was verified to be the dipole-dipole interaction.

A green-emitting phosphor of Eu^{2+}-doped $Ca_5(PO_4)_2SiO_4$ was prepared via a solid-state reaction by Roh et al [97]. The phosphor was excited at the wavelengths of 220 – 450 nm, which was suitable for the emission band of near-ultraviolet (n-UV) light-emitting diode (LED) (350 – 430 nm). In $Ca_5(PO_4)_2SiO_4:Eu^{2+}$ phosphor, there were three distinguishable Eu^{2+} sites, which resulted in a strong green emission peaking at 530 nm and broad bands up to 700 nm.

10.7. Catalysts

Catalysts are usually defined as the substances that increase the rate at which a chemical reaction approaches the equilibrium without becoming permanently involved in this reaction. Basically, the catalysis can be divided to [98]:

i. Homogeneous catalysis,

ii. Heterogeneous catalysis.

Heterogeneously catalyzed process is more complex because the catalyst is not uniformly distributed throughout the reaction medium. Considering a two-phase system, either vapor/solid or liquid/solid, with the catalyst in the solid phase, the several steps need to be realized to complete the catalytic cycle [98]:

1. Transport of the reactant to the catalyst;

2. Adsorption, i.e. the interaction of the reactant with the catalyst;

3. Reaction of adsorbed species to the products;

4. Desorption of the products from the catalyst;

5. Transport of the product away from the catalyst surface.

Due to their versatility in anionic and cationic composition and their ability to adsorb organic and organometallic molecules as well as metallic salts, the surface properties of apatites can be tuned and they can behave as powerful catalysts in a wide range of organic reactions. In many cases, the apatite-based catalysts can be used without a solvent and show good recycling capacity. The catalytic properties mainly arise from the acid-base character of the apatite's surface. In some cases, adsorbed moieties are responsible for the catalytic properties, apatites playing the role of a solid support. Finally, the catalytic activities can result from the combination of properties of the apatite's surface and of the adsorbed or anchored moieties [99].

The oxidative Glaser-Hay coupling reaction of terminal alkynes is a very important reaction in organic chemistry to achieve the synthesis of diyne compounds. In general, the reaction is performed under homogeneous conditions using Cu(I) or Cu(II) salts in the presence of a reagent such as tetramethylethylenediamine (TMEDA), which can bind to copper ions, an organic base and dioxygen. Although this reaction is known for a long time, the mechanism is still under the discussion. It is possible to catalyze the Glaser-Hay reaction under heterogeneous conditions using Cu-modified hydroxyapatite (Cu-HAp). With several para-substituted phenyl-acetylenes and alkynols, we can show that Cu-HAp acts as a catalyst for single-bond coupling reactions leading to diyne derivatives in high yields without using auxiliary chelating molecules and organic bases. These heterogeneous conditions allow easy recovery of the catalyst and simplify the purification work-up.

The oxidative Glaser-Hay coupling reaction of terminal alkynes (acetylenes) is a very important reaction in organic chemistry to achieve the synthesis of diyne compounds. In general, the reaction is performed under homogeneous conditions using Cu(I) or Cu(II) salts in the

presence of base (ethanolic ammonia solution, tetramethylethylenediamine, pyridine, …), which can bind to copper ions, an organic base and dioxygen [100],[101]:

$$R - C \equiv CH \xrightarrow[\text{base}]{\text{CuCl}} R - C \equiv C - C \equiv -R \tag{12}$$

Although this reaction is known for a long time, the mechanism is still under the discussion. It is possible to catalyze the Glaser-Hay reaction under heterogeneous conditions using Cu-modified hydroxyapatite (Cu-HAp). With several para-substituted phenyl-acetylenes and alkynols, where Cu-HAp acts as a catalyst for single-bond coupling reactions leading to diyne derivatives in high yields without using auxiliary chelating molecules and organic bases. These heterogeneous conditions allow easy recovery of the catalyst and simplify the purification work-up [100].

The apatite catalyst was utilized for the catalysis of the synthesis of n-butanol, 1,3-butadiene and high octane fuel from bioethanol. The process requires relatively low temperature. The synthesis shows significantly lower cost compared to n-butanol derived from petroleum-based processes. The technology offers a closed-loop system with no waste or emissions [102].

10.8. Phosphate conversion coatings

Conversion coatings provide the resistance to corrosive environments. Phosphate conversion coatings (PCC) bring about the transformation of metal substrates into new surfaces having non-metallic and non-conducting properties. The transformations occur in phosphating solution containing divalent metal phosphates and, in some cases, in solutions containing monovalent metal phosphates. Generally, the solutions are prepared from liquid concentrates containing one or more divalent metals (zinc, magnesium, calcium, etc., phosphates), free phosphoric acid and an accelerator. Three types of phosphate conversion coatings are currently being used [103],[104]:

1. **Zinc phosphate coatings** are often used as a pretreatment for painted parts. They are also used to impart the corrosion resistance and to aid in cold-forming operations.
2. **Iron phosphate coatings** are primarily used to form a passive substrate under paints.
3. **Manganese phosphate coatings** are primarily on machined parts such as gears and internal combustion engine components as an anti-scuff film for the break-in wear.

The addition of metal ions, such as cupric ions, to a conversion bath greatly reduces the formation time and the size and nonuniformity of coating crystals. Copper, which is cathodic to dissolving metals, deposits on the base metal to form many local cells and thus to increase the potential difference between local anode and cathode site. Nickel ions behave differently than cupric ions, and their benefit results from the catalytic action associated with the release of molecular hydrogen. Furthermore, the addition of Ni^{2+} and Mn^{2+} into the treating solution

refines the grain size and reduces the porosity of phosphate conversion coatings on electro-galvanized steels. While Ni exists in both the zero-valance state and the two-valance state, Mn is mainly present in the two-valance state in the phosphate conversion coating [103],[105].

In fact, all of the chemical reactions of phosphating process are based on mutual interactions of metal immersed in phosphate bath and redox of the accelerators. Generally, phosphating proceeds in the acidic solution containing Zn^{2+}, Mn^{2+}, Ca^{2+}, Na^{+}, Fe^{2+} and Mg^{2+}. Phosphating with different metal substrates and types is not of the same reaction mechanism. For example, when a pure iron is immersed in the phosphating solution, iron dissolves on the micro-anodes through the following reaction [106]:

$$Fe + 2\ H^{+} \rightarrow Fe^{2+} + H_2 \tag{13}$$

The hydrogen evolution occurs at the micro-cathodic sites resulting in an increase of pH value at the metal-solution interface. This change in pH alters the dissociation equilibrium, which leads to the formation of PO_4^{3-}:

$$H_3PO_4 \rightarrow H_2PO_4^{-} + H^{+} \rightarrow HPO_4^{2-} + 2\ H^{+} \rightarrow PO_4^{3-} + 3\ H^{+} \tag{14}$$

When PO_4^{3-} and Me^{2+} (metal ion, e.g. Zn^{2+}, Mn^{2+}, Ca^{2+} and Fe^{2+}) in the solution reach the saturation, the deposition of insoluble phosphate will be achieved. Then, it can crystallize in PCC coating, as shown in **Fig. 12**.

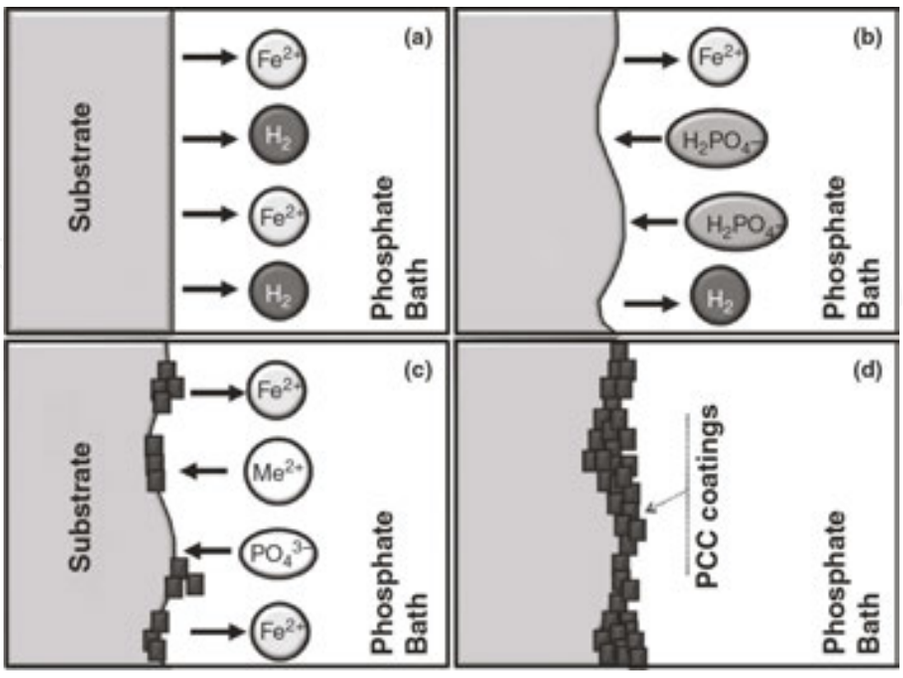

Fig. 12. Schematic representation of the deposition process of PCC coating on the surface of pure iron [106].

In the zinc phosphating solution, the addition of Zn^{2+} supports the formation of crystals of zinc phosphate. Zinc ions combine with phosphate ions to form an insoluble film. The formation of hopeite is described by the reaction [106]:

$$\begin{aligned} &3\ Zn^{2+} + 2\ H_2PO_4^- + 2\ H^+ + 4\ H_2O + 6\ e^- \rightarrow \\ &Zn_3\left(PO_4\right)_2 \cdot 4H_2O + 3\ H_2 \end{aligned} \tag{15}$$

In some cases, Zn and ZnO were found in the phosphating process in reactions:

$$Zn + 2\ e^- \rightarrow Zn \tag{16}$$

$$Zn + 2\ H_2O \rightarrow Zn\left(OH\right)_2 + H_2 \tag{17}$$

$$Zn\left(OH\right)_2 \rightarrow ZnO + H_2O \tag{18}$$

In the phosphate solution of coexisting Zn^{2+} and Ca^{2+}, zinc calcium phosphate can be formed by the reactions:

$$Ca^{2+} + HPO_4^{2-} \rightarrow CaHPO_4 \tag{19}$$

$$Ca^{2+} + 2\ Zn^{2+} + 2\ H_2PO_4^- + 2\ H_2O \rightarrow CaZn_2\left(PO_4\right)_2 \cdot 2H_2O + 4\ H^+ \tag{20}$$

It is notable that the phosphating mechanism varies in different phosphating systems and materials [106].

The formation of conversion coating on zinc-coated samples under cathodic conditions was studied by Perrin et al [107] in a chromating bath containing phosphate (phosphate-chromate solution). Thick chromium phosphate (Cr-P) coating has two distinct layers: an outer porous layer and an inner and thinner pore-free adherent one. Both layers contain chromium phosphate as the main constituent and, to a lower extent, zinc phosphate species, the concentrations of which decrease from the metal-coating interface outwards. Formed zinc phosphates have a general formula of $\boldsymbol{x}CrPO_4 \cdot \boldsymbol{y}Zn_3(PO_4)_2 \cdot \boldsymbol{z}\ H_2O$ where $\boldsymbol{x} > (\boldsymbol{y}, \boldsymbol{z})$.

10.9. Synthetic apatite analogues in tissue engineering

Biomaterials in general are based on the materials such as metals, polymers, and ceramics. Typical metallic biomaterials are based on stainless steel, cobalt-based alloys, titanium or

titanium alloys and amalgam alloys. Polymeric biomaterial composites from monomers are based on amides, ethylene, propylene, styrene, methacrylates and/or methyl methacrylates. Biomaterials based on ceramics are found within all classical ceramic families (**Table 3**) including traditional ceramics, special ceramics, glasses, glass-ceramics, coatings and chemically bonded ceramics (CBCs) [13].

Ceramic material classification	Example
Traditional ceramics	Dental porcelain, leucite-based ceramics
Special ceramics	Al, Zr and Ti oxides
Glass	Bioglass (Na_2O-CaO-P_2O_5-SiO_2)
Glass-ceramics	Apatite-wollastonite, Li-silicate-based
CBCs	Phosphates, aluminates, silicates and sulfates

Table 3 Examples of biomaterials based on ceramics [13].

Whereas many chemists and materials scientists consider the biomaterial to be synthetically produced material, most biologists, geologists and mineralogists consider the materials such as bone and tooth, which are biologically produced, to be the biomaterials. Also a common reference to Ca:P (1.67, **Table 7** in **Chapter 1**) ratio is usually used in the biomaterials literature, which disregards the fact that different calcium phosphate phases have different crystalline structures.

There are many phosphate minerals and salts (**Table 4**) that do not have the crystalline structure of apatite [108],[109]. Apatite-based materials have attracted a considerable interest for orthopedic and dental applications because of their biocompatibility and tight bonding to bone, resulting in the growth of healthy tissue directly onto their surface. Several combinations of apatite and other phases were proposed in order to improve poor mechanical properties of apatite [110].

Typical acronym	Chemical name	Chemical formula	Mineral name	Structure	Ca/P ratio
HAP, HA	Tribasic calcium phosphate	$Ca_5(PO_4)_3OH$	Hydroxylapatite	Apatitic	1.67
ACP	Amorphous calcium phosphate	?	—	—	?
PCHA, PCA	Poorly crystalline hydroxylapatite	$Ca_5(PO_4)_3OH$	Hydroxylapatite	Apatitic	1.67
CAP	Carbonated apatite	Refer to **Sections 2.6** and **4.6**			
TCP	Tricalcium phosphate	$Ca_9(PO_4)_6$	Whitlockite	Non-apatitic	1.5
β-TCMP	Magnesium-substituted TCP	$Ca_9(PO_4)_6$	Whitlockite	Non-apatitic	≤1.5

Typical acronym	Chemical name	Chemical formula	Mineral name	Structure	Ca/P ratio
?	"Tricalcium phosphate"	$Ca_9(Mg,Fe^{2+})(PO_4)_6(HPO_4)$	Geologically occurring whitlockite	Non-apatitic	1.28
CPPD	Calcium pyrophosphate dihydrate	$Ca_2P_2O_7{\cdot}2H_2O$	—	Non-apatitic	1.0
γ-CCP	γ-Calcium pyrophosphate	$Ca_2P_2O_7$	—	Non-apatitic	1.0
OCP	Octacalcium phosphate	$Ca_8H_2(PO_4)_6{\cdot}5H_2O$	—	Non-apatitic	1.33
MON	Dibasic calcium phosphate	$Ca(HPO_4)$	Monetite	Non-apatitic	1.0
DCPD	Dicalcium phosphate dihydrate	$Ca(HPO_4){\cdot}2H_2O$	Brushite	Non-apatitic	1.0

Table 4 Different apatitic and non-apatitic calcium phosphates [108].

Small organic molecules incorporated in apatite crystals act as porogens that control the porous structure of apatite single crystal. The presence of amino acid under the apatite synthesis conditions leads to firm bindings and encapsulation of amino acid within apatite single crystals. The amino acid elimination by heating or electron beam irradiation enhances the pore formation in apatite single crystals. Moreover, the incorporation of acidic amino acid into apatite induces the peapod-like nanotubes in apatite single crystals. That suggests the potential of using small organics for nanostructural control of apatite single crystals, which would be valuable for enhancing the drug loadings or for modulating the material digestion in vivo [111].

10.9.1. Biological apatite in bone tissue engineering

Tissue engineering (TE) techniques were developed to recover or enhance lost tissue function and structure. In biological hard tissues, for example, lost portions can be effectively reconstructed by the control of environmental factors, physical stimulation, addition of growth factors and by the use of degradable materials. These factors strongly facilitate the regeneration of macroscopic shape of defected hard tissues. Nevertheless, the differences in microstructure, and also in mechanical and physical properties, between regenerated and original hard tissues must be examined prior to clinical application [112],[113],[114].

For in vitro engineering of living tissues, cultured cells are grown on bioactive degradable substrates (scaffolds[8]) that provide the physical and chemical cues to guide their differentiation and assembly into three-dimensional structures. One of the most critical issues in TE is the realization of scaffolds with specific physical, mechanical and biological properties. Scaffolds act as substrate for cellular growth, proliferation and the support for new tissue

[8] Scaffolds might be defined as artificial structure capable of supporting the three-dimensional tissue formation, which allows the cell attachment and migration, the delivery and retaining of cells and biochemical factors and enables the diffusion of vital cell nutrients and expressed products. In the case of bone, scaffolds should replicate its architecture and three-dimensional structure with predetermined density, hierarchical pore distribution and interconnected pathways [109],[115].

formation. Biomaterials and fabrication technologies play a key role in tissue engineering. Materials used for tissue engineering applications must be designed to stimulate specific cell response on the molecular level. They should elicit specific interactions with the cell and thereby direct cell attachment, proliferation, differentiation and extracellular matrix production and organization [109],[115]:

- **Biocompatibility** is defined as the ability to perform its function in the host tissue without eliciting any immune response.
- **Biodegradability** denotes tunable rate of degeneration to match the growth of new bone tissue as scaffold gets replaced by new bone.
- **Mechanical properties** include the properties such as sufficient mechanical strength to provide temporary support to the defect region and withstand in vivo loading forces.
- **Microarchitecture** is an interconnected scaffold structure that uniformly distributes stresses throughout the scaffold.
- **Osteoinductivity** includes osteoinductive properties that enable to recruit and differentiate the osteoprogenitors to the defect region.
- **Porosity** is large surface area, where the volume and the pore size allow the tissue in-growth, neovascularization, mass transport and the osteogenesis.
- **Surface properties** include appropriate chemical and topographical properties for influencing cellular adhesion, proliferation and differentiation.

Inorganic-organic composites aiming at mimicking the composite nature of real bone combine the toughness of the polymer phase with the compressive strength of an inorganic one to generate bioactive materials with improved mechanical properties and degradation profiles. Hydroxylapatite (HAP) is widely used as a biocompatible ceramic material in many areas of medicine, but mainly for the contact with bone tissue, due to its resemblance to mineral bone [115].

Under normal conditions, human body fluid is supersaturated with respect to apatite, so that, when apatite nuclei form, crystals can grow spontaneously. Chemical species that are capable of supporting the nucleation of apatite are calcium and silicate ions, while, in contrast, phosphate ion does not affect this process. Hence, ceramics that release the former mentioned ions are capable of developing the surface apatite layer when exposed to human body fluids. This explains why glasses that do not contain P_2O_5 are able to develop this surface layer and show greater bioactivity than glasses containing P_2O_5, even if the latter compositions approximate to that of hydroxyapatite [116].

10.9.2. Preparation of nanocrystalline apatites

Nanocrystalline calcium phosphate apatites play an important role in biomineralization[9] and in the field of biomaterials. Biological nanocrystalline apatites are the main inorganic compo-

[9] The enamel of vertebrate teeth, vertebrate bone and tooth-like microfossils of conodonts.

nents of hard tissues in mammals (bone[10] and tooth[11] (**Fig. 13**)) with the exception of enamel (which is closer to stoichiometric hydroxylapatite) and are involved in several pathological calcifications such as dental calculi, salivary stones and blood vessel calcification. In comparison with hydroxylapatite, which is a stoichiometric apatitic phase and is the most stable and the least soluble calcium phosphate at ambient conditions, nanocrystalline apatites are nonstoichiometric and calcium (and OH-) deficient and may incorporate substituted ions in their nanosized crystals. Their calcium and hydroxide deficiencies are responsible for higher solubility than HA. Besides, they have the ability to mature when submitted to humid environments [108],[112],[117],[118].

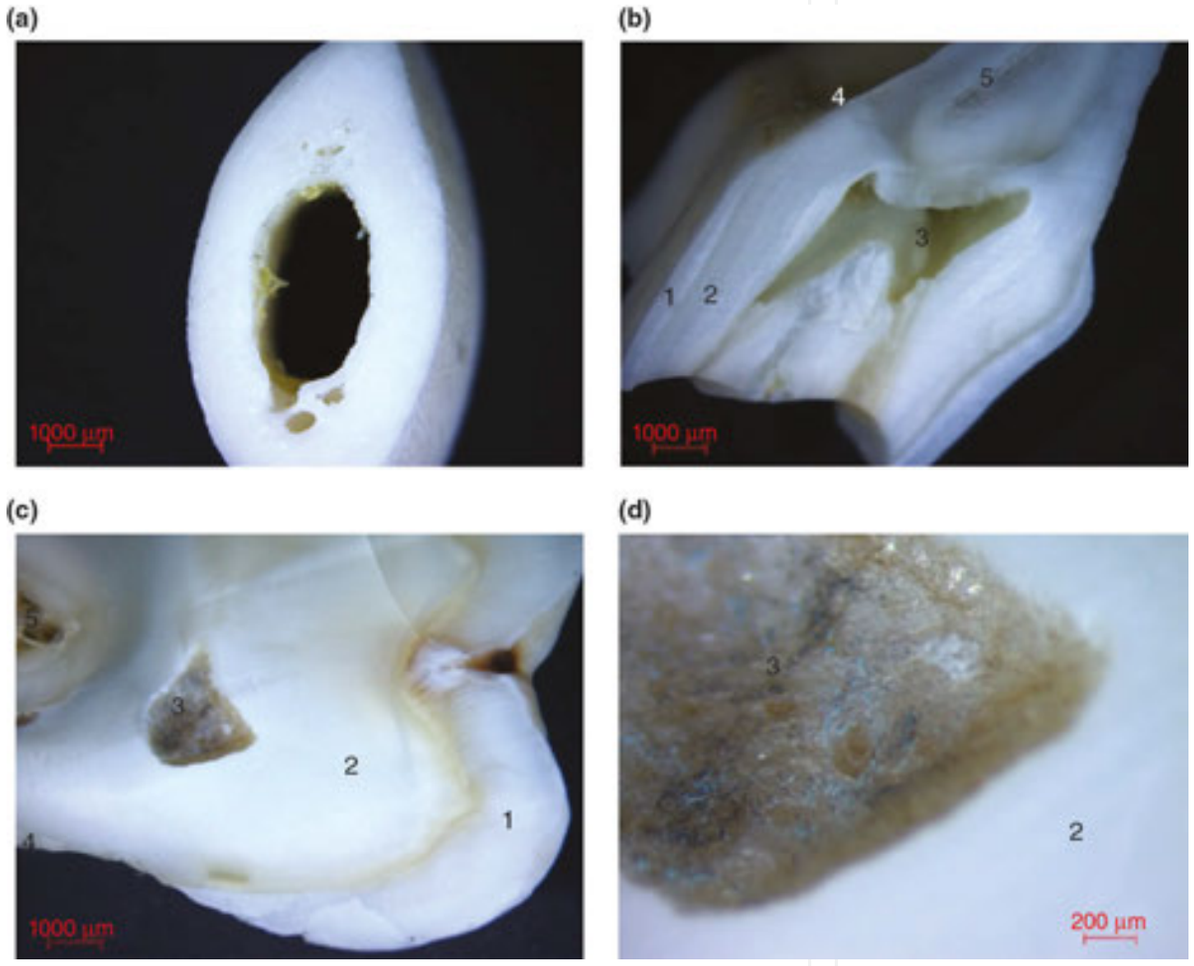

Fig. 13. The cross-section of lower jaw bone (a) and tooth (b) of European roe deer (*Capreolus capreolus*) and human tooth (c, d): enamel (1), dentin (2), pulp chamber (3), cementum (4) and root canal (5).

[10] Bones are rigid organs that form a part of the endoskeleton of vertebrates. Their function is to move, support and protect various organs of the body, produce red and white blood cells and store minerals. Bones appear in a variety of shapes and have a complex internal and external structure described by various hierarchical models [117]. Bone is a complex and hierarchical tissue consisting of nano-hydroxylapatite (70 wt.%) and collagen (30%) as major portions [113].

[11] Teeth consist of a bulk of dentin covered with (inorganic) enamel on the crown and cementum on the root surface. Thick collagen bundles, called periodontal ligaments (PDL), attach to cementum at one end and to the alveolar bone at the other end. The alveolar bone is supported by the jaw [117].

http://dx.doi.org/10.5772/62217

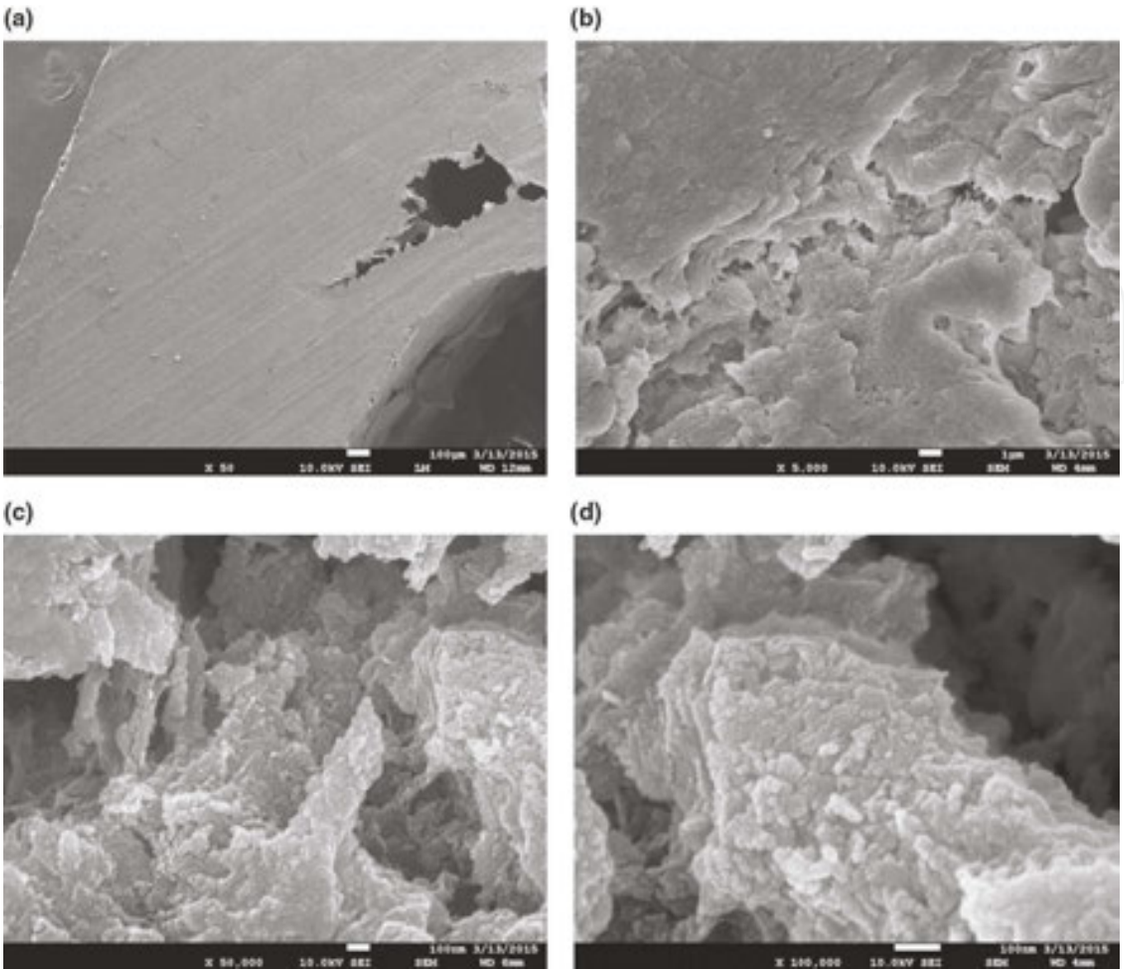

Fig. 14. Electron microscopy picture (SEM) of lower jawbone of European roe deer from **Fig. 13** under magnification of 50× (a), 5000× (b), 50,000× (c) and 100,000× (d).

Scanning electron microscopy of deer bone (**Fig. 14**) shows a spongiform texture (*a*, *b*) formed by crystals of carbonated hydroxylapatite with the size below 100 nm (*e*, *f*).

The inorganic portion of bone contains two major mineral phases

i. Non-crystalline calcium phosphate;

ii. Crystalline bone apatite.

In amorphous calcium phosphate, the Ca:P ratio is about 1.33. The non-crystalline or amorphous bone mineral is metastable with respect to bone apatite. Bone apatite crystals are calcium deficient due to the defects in the crystalline lattice and isomorphous substitutions, that is, the replacement of some ions by others in the crystal without disrupting the general symmetry. Young bone tissue was found to be richer in amorphous mineral than crystalline apatite [119].

In the body, only the bone collagen has the property of inducing the mineralization through in vitro; collagens of other tissues do not possess this property. One of the differences between nucleating and non-nucleating collagens might be the presence of a sort of inhibitor bound to

the latter. This inhibiting substance was shown to be pyrophosphate. Calcium is accreted in bone tissue in the process of new bone formation or remodeling and resorbed from the bone tissue in the process of bone destruction. The loss of endogenous calcium in urine and feces is compensated for by an equivalent intake of this element (**Fig. 15**) [119].

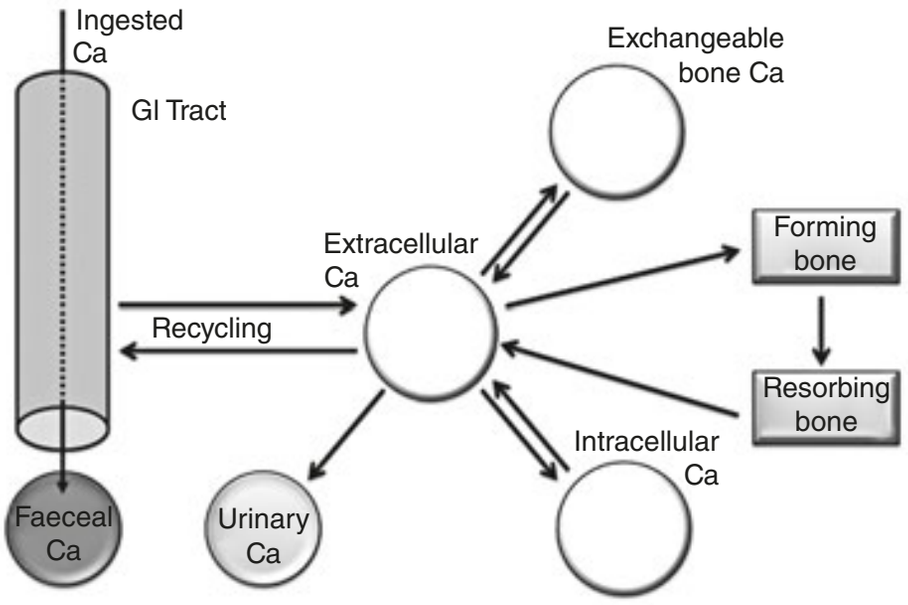

Fig. 15. General scheme of metabolism of calcium [119].

Enamel (**Fig. 17**) is normally the best preserved from hard tissues. It is almost completely a mineral, so the decomposition of organic matter has little effect on it. Archeological enamel nearly always yields good microscope sections, often indistinguishable from fresh enamel [120]. The structure of carbonate dental enamel refined by Wilson et al [121] is shown in **Fig. 16**.

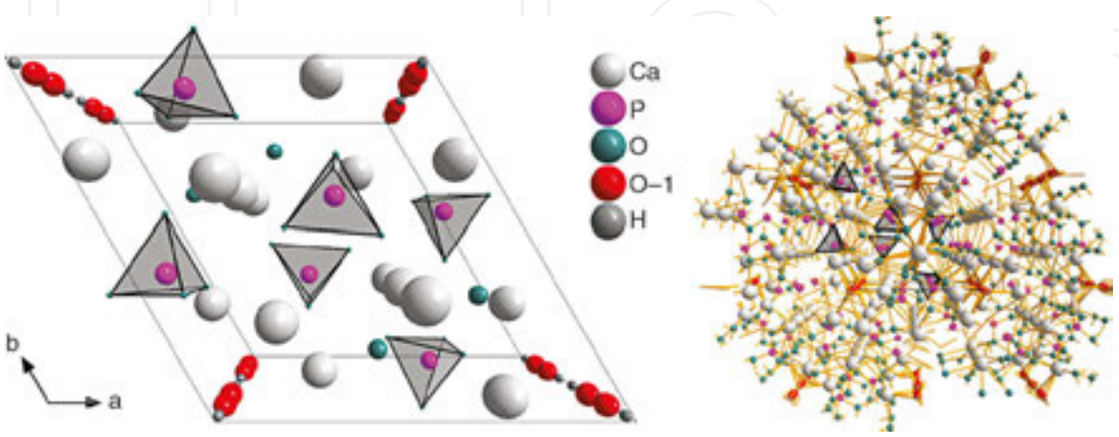

Fig. 16. Crystallographic structure of human dental enamel apatite (perspective view along the c-axis): $P6_3/m$, a = 9.4081 Å, b = 6.8887 Å, c:a = 0.7322 and V = 528.05 Å^3 [121].

http://dx.doi.org/10.5772/62217

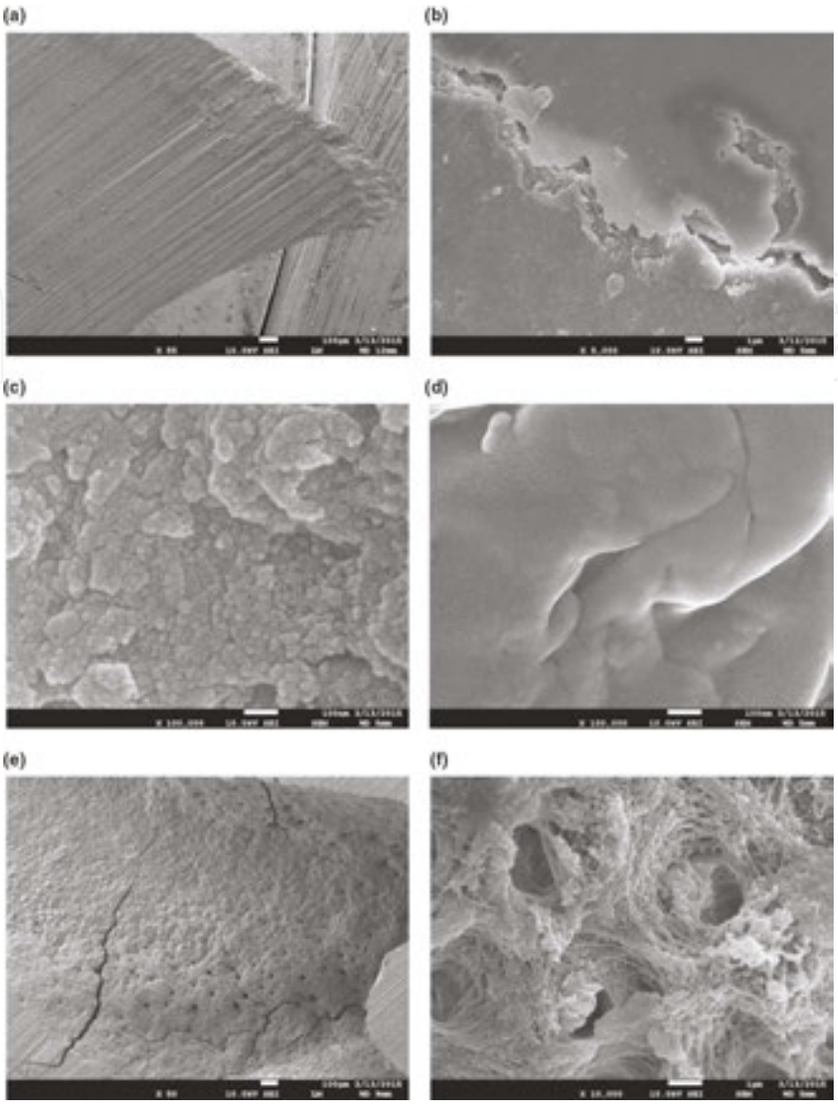

Fig. 17. Electron microscopy picture (SEM) of tooth from **Fig. 13**: the crown with enamel-dentin interface (*a*, *b*), nanocrystals of carbonated hydroxylapatite in the texture of dentin (*c*), glass-like texture of enamel (*d*) and surface of pulp chamber (*e*, *f*).

Among carbonate apatites, which are formed in mouth cavity, only dental enamel mine belongs to the B-type of carbonate-apatite (**Section 4.6**) and the others (of dentin, salivary and dental stones) belong to the AB-type (B > A). According to the variations in unit-cell parameters, isomorphic replacements in crystal structures of apatites of pathogenic origin (renal, salivary and dental stones) are more intensive in comparison with physiogenic dental enamel apatites. Among pathogenic apatites, the most considerable compositional variations are observed in renal stone apatites. That indicates strong variability of conditions of their formation. The changes in unit-cell parameters of bone apatites are not completely interpretable, because these apatites consist of nanosized crystals that are smaller than those of other biological apatites [122].

The age variations of the crystal lattice parameters of human enamel apatites are related to complicated processes of de- and remineralization, which result in the increase or reduction of vacancies in Ca positions and in the respective changes of CO_3^{2-}, H_2O and HPO_4^{2-} contents in the unit cell:

$$\begin{aligned} &\left(n+m/2\right)\ Ca^{2+}n\ PO_4^{3-}+m\ OH^- \rightarrow \\ &\left(n+m/2\right)\left[\ \right]_{Ca}+n\ A^{2-}+m\left(\left[\ \right]_{OH^-},H_2O\right) \end{aligned} \tag{21}$$

where $A^{2-} = CO_3^{2-}$ or HPO_4^{2-}, and $[]_{Ca}$, $[]_{OH-}$ are the vacancies. Until the age of 50 years, the values of ***a*** and ***c***-parameter of enamel apatites change considerably without any dependence of particular age that may be explained by essential fluctuations of the content of Ca in human organism. After 50 years of age, significant direct correlation between the age and the ***a***-parameter appears [122].

The surface of apatite nanocrystals is possibly doped with foreign elements or functionalized with organic molecules [117],[123],[124]. The course of facile synthesis of B-type carbonated nanoapatite with tailored microstructure is described by Gualtieri et al [125].

10.10. Collagen apatite composites

Tissue engineering techniques have been developed to recover or enhance lost tissue function and structure.[12] Collagen-apatite[13] (or collagen/apatite, **Col-AP**) composite resembling the composition of natural bone[10] has been studied extensively and considered as a promising bone tissue engineering material, which can be used to replace or regenerate damaged tissue, resulting from an accident, trauma or cancer. Such synthetic or hybrid biomaterials must have high porosity with interconnected pores to allow the vascularization as well as the nutrients and gases diffusion. Moreover, they should be biodegradable to act as temporary cellular support [114],[126],[127],[128].

The defining feature of collagen is a structural motif in which three parallel polypeptide strands in a left-handed, polyproline II-type (**PPII**) helical conformation coil around each other with a one-residue stagger to form a right-handed triple helix. Tight packing of **PPII** helices within the triple helix mandates that every third residue be **Gly**, resulting in a repeating **XaaYaaGly** sequence, where **Xaa** and **Yaa** can be any amino acid. This repeating occurs in all types of collagen, although it is disrupted at certain locations within the triple-helix domain of nonfibrillar collagens. The amino acids in the **Xaa** and **Yaa** positions of collagen are often (2S)-

[12] One of the first polymers used for bone tissue engineering was based on a hydrolytically copolymer of polylactic-co-glycolic acid (PLGA) but its use for large bone defect regeneration was controversial as inflammatory events were observe. The utilization of chitosan and alginate was also investigated [128].

[13] Names such as collagen-hydroxylapatite or collagen-hydroxyapatite composite were also often applied in published literature.

proline (**Pro**, 28%) and (2S,4R)-4-hydroxyproline (**Hyp**, 38%), respectively. The **ProHypGly** is the most common triplet (10.5%) in collagen (**Fig. 18**) [129].

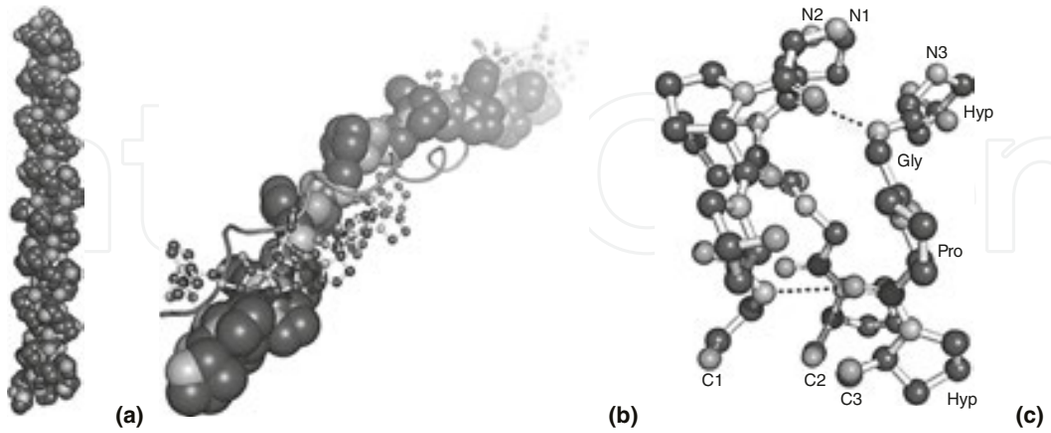

Fig. 18. The triple helix of collagen formed from $(ProHypGly)_4$-(ProHypAla)-$(ProHypGly)_5$ (a), the view down the axis of a $(ProProGly)_{10}$ triple helix (b) and the segment of triple helix (c) with hydrogen bonds (—) [129].

The categories of collagen[14] include the classical fibrillar and network-forming collagens, the FACITs (fibril-associated collagens with interrupted triple helices), MACITs (membrane-associated collagens with interrupted triple helices) and MULTIPLEXINs (multiple triple-helix domains and interruptions). The collagen of type I is the most abundant type used in tissue engineering. Natural polymer collagen that represents the matrix material of bone, teeth and connective tissue can be extracted from animal or human sources (skin, bones, tendons, ligaments and cornea). The treatment includes the separation and isolation (in soluble or insoluble form), decalcification, purification (purification is required to eliminate the antigenic component of protein), sterilization and chemical modification process to achieve polyanionic or purified protein. Type I polyanionic collagen was found to improve the cell adhesion [129],[130].

Collagen, the most abundant protein in extracellular matrix, is chemotactic to fibroblasts. It shows high affinity to cells and good resorbability in vivo. Nevertheless, its poor mechanical properties have restricted its usage in load-bearing applications. Carbonated apatite and collagen interact to form a composite material, the mechanical, physicochemical and biological properties of which differ considerably from those of either constituent considered separately. Collagen and non-collagenous proteins (**NCPs**) are thought to control the crystal deposition, size, crystallization and multiplication/maturation. On the other hand, the crystal deposition in intrafibrillary spaces is likely to modify the three-dimensional conformation of collagen [114],[131],[132],[133]. The solubility of apatite-collagen composites is significantly reduced by UV radiation [134],[135].

[14] There are 27 types of collagen described in literature composed of at least 46 distinct polypeptide (CRP, collagen-related peptide) chains [129], but the types I – V are the most common. More than 90% of collagen in human body is the fibrillar type I.

Calcium phosphates are available commercially, as hydroxylapatites are extracted from bones or they can be produced wet by direct precipitation from pH-adjusted solutions of calcium and phosphate salts [130]. The crystallographic c-axes of the plate-shaped apatite crystals are well aligned with long axes of collagen fibrils (**Fig. 19**), and this preferred orientation between the mineral and the organic framework is assumed to be the general feature of the calcium phosphate biomineralization process. Several attempts were made to mimic this lowest level of hierarchical organization of bone by using proteins as a site for the heterogeneous nucleation and subsequent growth of stoichiometric hydroxylapatite crystals. In special approaches, the biomimetic apatite coatings on surfaces were prepared by soaking the materials in simulated body fluid (SBF) solutions, which contained ions in the concentrations similar to those in inorganic part of human blood plasma. It is generally accepted that the in vitro apatite growth during the exposure to SBF is an indicator for the in vivo bioactivity of materials surface [136],[137].

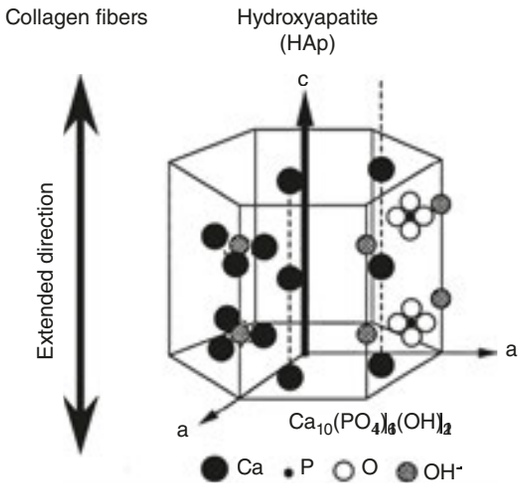

Fig. 19. The crystal structure of hydroxylapatite is oriented according to the c-axis with the extended direction of collagen fibrils [112].

Biomimetic materials are able to mimic the morphological and physicochemical features of biological apatite compounds, i.e. they are synthetic analogues of inorganic part of hard tissues [112],[117]. The biomimetic deposition is considered as an ideal method to produce calcium phosphate ceramics such as apatite coatings on titanium and its alloys for medical applications. It has also been proved that the chemical pretreatment in alkali solution can improve the bonding between the titanium substrate[15] and calcium phosphate coatings fabricated by subsequent biomimetic deposition in simulated body fluid (SBF) [138],[139], [140],[141]. The biomimetic growth of apatite was also described on hydrogen-implanted silicon [142], polyvinyl alcohol (PVA) [143], TiO_2 nanotubes [144], alumina [145], zirconia ceramics (Y-TZP) [146], forsterite [147], akermanite [148], magnetite [149], glasses [150] and

[15] Titanium and its alloys are widely used as orthopedic and dental implant materials because of their high mechanical strength, low modulus and good corrosion resistance [139].

bioglasses [151],[152], cements [153], geopolymers [154], carbon nanotubes [155] and microspheres [156].

The ability to form apatite [150],[153] from supersaturated solution has been widely used to imply the bioactivity of an implant in vivo. However, the method itself may provide at best incomplete information, primarily because it is determined only by the solution supersaturation, irrespective of biological processes. The bone regeneration is triggered mainly by the vitality of osteoblasts and regulated by the expression of growth factors such as estrogen, parathyroid hormone and bone morphogenetic proteins, while ions or other species released from an implant may affect the expression of such growth factors and so the bone resorption or formation. The misinterpretation of the outcome of such tests must result in the misunderstanding of the true effects and behavior of materials intended for use in embedded biological applications. Moreover, SBF may not be able to mimic properly the physiological conditions because it is based on analytical concentrations and not on the activity of key components [157].

The methods of the preparation of collagen-hydroxylapatite composites include the production of composite gels, films, collagen-coated ceramics, ceramic-coated collagen matrices and composite scaffolds for bone substitutes and hard tissue repair via the following techniques [130],[158],[159]:

- **In vitro collagen mineralization**: the method is based on direct mineralization of a collagen substrate (film) through which calcium and phosphate ions diffuse into the fibrils or as phosphate-containing collagen solution[16] (in situ precipitation [159]). **Fig. 20** introduces the experimental set-up for direct mineralization of a collagen sheet. The growth of HAP crystals with c-axis oriented along the collagen fibrils requires the pH in the range from 8 to 9 and the temperature of 40°C. These conditions promote the accumulation of calcium ions on the carboxyl groups of collagen molecules, leading to the nucleation of hydroxylapatite.

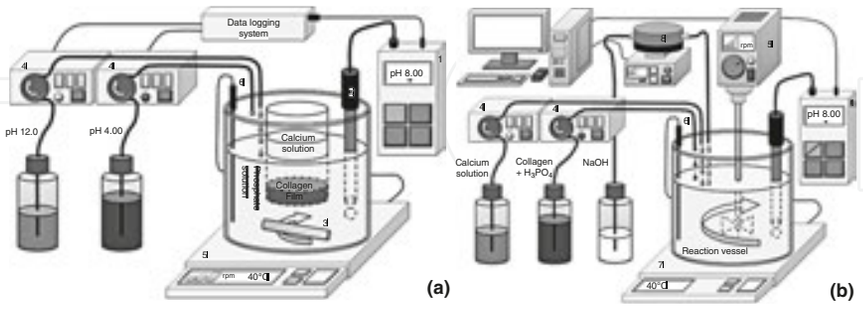

Fig. 20. Simplified scheme of apparatus for the preparation of collagen-hydroxylapatite composite by in vitro collagen mineralization method: modified scheme according to Wahl and Czernuszka [130] for in situ collagen/HAP precipitation (*a*); modified scheme according to Wang and Liu [159]: pH meter (1), pH electrode (2), stirrer (3), peristaltic pump (4), hot-plate magnetic stirrer (5a) or stirrer (5b), thermocouple (6), hot plate (7) and peristaltic pump driven by pH controller (8) (b).

[16] These techniques usually continue with freeze-drying.

- **Thermally triggered assembly of HA/collagen gels**: the solution of calcium and phosphate ions is encapsulated within the liposomes and next inserted into the acidic suspension of collagen. After the injection into a skeletal defect, the increasing temperature due to body heat initiates the gelation process, which leads to fibrous network. The mineralization occurs after reaching the liposome's transition temperature of 37°C.
- **Vacuum infiltration of collagen into a ceramic matrix**: ceramic scaffold is prepared by heating aqueous hydroxylapatite slurry containing poly(butyl methacrylate) (PBMA) spheres to high temperatures. The pyrolysis of PBMA particles leads to porous HAP green body. Pores in this matrix are then filled with collagen suspension under vacuum. The final composite was then freeze-dried to produce the microsponges within.
- **Enzymatic mineralization of collagen sheets**: is a method based on the cycle (**Fig. 21**) where collagen-containing alkaline (basic) phosphatase (ALP) is treated by aqueous solution of calcium ions and phosphate ester. The enzyme provides a reservoir for PO_4^{3-} ions for calcium phosphate to crystallize and the mineralization occurs on coated area. The sample is then coated again with collagen suspension, air-dried and cross-linked with UV irradiation. Repeating this cycle results in multilayered composite sheets of calcium/phosphate and collagen.

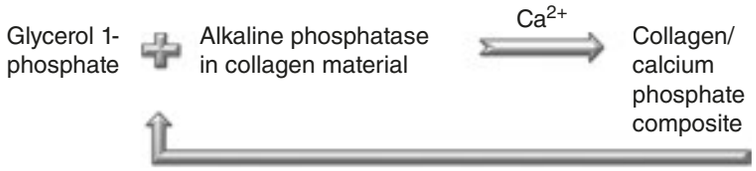

Fig. 21. The cycle of enzymatic mineralization of collagen sheets [130].

- **Water-in-oil emulsion system**: purified collagen suspension mixed with HAP powders at the temperature of 4°C is next dispersed in olive oil and stirred at 37°C. The collagen aggregates and reconstitutes into the aqueous droplets. The addition of phosphate-buffered saline[17] (PBS) leads to the gelation of Col-HAP microspheres (gel beads) of bone filler. The main disadvantages of this method are the problem with complete removing of the oil content from the composite and too low viscosity of the mixture.
- **Freeze-drying and critical point drying (CPD) scaffolds**: the ice crystals with collagen fibers at the interstices can be formed by freezing the suspension of collagen and HAP in water under controlled conditions. In the case when the freeze-drying is applied (temperature and pressure corresponding to CPD), ice crystals sublimate to water vapor.

  Under the condition of critical point,[18] the density of liquid and gas phase converge and become identical (supercritical fluid) as well as the surface tension is negligible.

[17] Aqueous solution of sodium phosphate and chloride, where the ion concentrations and osmolarity (osmotic concentration) correspond to human body. In some cases, potassium phosphate and chloride were used.

[18] Critical point is defined by the value of three parameters including critical temperature, critical pressure and critical volume. Critical temperature is the highest temperature at which pure matter can exist as liquid.

- Col-HAP was cast into the mould and frozen, ice crystals replaced with ethanol, ethanol-liquid CO_2 exchanged and critical point dried to finally arrive with an exact porous replica of the original bone. Solid freeform fabrication techniques have recently been developed with artificial polymers and ceramic materials. These have the ability to change the pore interconnectivity, pore size and pore shape but have the disadvantage of not having the affinity of collagen to cell attachment. Another major advantage of Col-HAP scaffolds produced through the SFF method is the ability to control variables such as the control of external and internal structure, porosity and cross-linking [130].

The collagen-hydroxyapatite/pectin (Col-HA/pectin) composite was prepared in situ by the introduction of pectin, a kind of plant polysaccharide, into the collagen-hydroxyapatite composite. The structure of composite consisted of hydroxylapatite of low crystallinity with particles uniformly dispersed in organic materials. There is strong bonding interaction between HAP, collagen and pectin. The mechanical properties, water absorption, enzyme degradation and cytotoxicity indicate a potential use in bone replacement for the new composite [160].

Most mammalian biofluids are supersaturated with respect to the bone and tooth mineral hydroxylapatite. Nevertheless, the biofluids, which are in contact with soft tissues, especially those like milk that must be stored for any length of time, should be highly stable with respect to calcium phosphate precipitation. In contrast, saliva and the extracellular matrix of hard tissues, especially near to the sites of mineralization or remineralization, are required not only to maintain the mineral phase with which they are in contact but also to deposit calcium phosphate in a highly controlled manner [161].

Collagen composites were also used as a scaffold for the repair of soft tissues. These materials provide analogous environment to extracellular matrix (ECM) and induced rate of synthesis or growth of new tissues. Several natural polymers as collagen, chitosan,[19] gelatin[20] and keratin[21] possess the ability to induce the proliferation of cells and hence find their use as biomaterials for a wide range of biomedical applications. Among all biopolymers, collagen is a widely accepted material for the tissue engineering applications in the view of its low antigenicity, excellent biocompatibility and biodegradability [162].

The preparation of collagen-based biocomposite constructed from micro-crimped long collagen fiber bundles extracted from a soft coral embedded in alginate hydrogel matrix was described by Sharabi et al [163]. This biocomposite demonstrated the hyperelastic behavior similar to human native tissues.

[19] Chitosan is (1–4)-linked 2-amino-2-deoxy-b-glucan, a byproduct of N-deacetylation of chitin. It is a major constituent of crab and shrimp shells and of cuticles of insects.

[20] Gelatin is a denatured form of collagen. Gelatin has low antigenicity and promotes the cell adhesion, differentiation and proliferation. Gelatin also possesses high cytocompatibility, which makes it a potential candidate as a biomaterial for various tissue engineering applications [162].

[21] Keratin is a family of fibrous proteins, which is found abundantly in nature. It is the main constituent of hair, wool, nails, horns and hooves of mammals, birds and reptiles [162].

10.11. Layers and biocoatings

The nanostructured coatings are expected to enhance the mechanical properties and improve the strength of bonding between coating and implant. These materials can also promote the deposition of calcium-containing minerals on their surface (bioactivity). Some typical examples of the research carried out in recent years, in the field of fabrication of nanostructured glass-ceramic coatings, utilize various techniques such as conventional enameling, sputtering, sol-gel processing, ion beam deposition, plasma spraying, electrophoretic deposition and pulsed laser deposition [164].

As was mentioned earlier, among the bioactive ceramics, the apatite/wollastonite (A/W) glass-ceramics, containing apatite and wollastonite crystals in the glassy matrix, has been largely studied because of good bioactivity and was used in some fields of medicine, especially in orthopedics and dentistry. However, medical applications of bioceramics are limited to non-load-bearing applications because of their poor mechanical properties. The solution of this problem can be the preparation of layers on the titanium alloy base material. Thermally sprayed layers by APS (atmospheric plasma spraying) on Ti-6Al-4V substrates combine good bioactivity of the bioceramics and good mechanical strength. The microstructure and the resulting properties were evaluated depending on the processing parameters and postprocessing thermal treatments. Thermal treatments decreased the bioactivity of the coatings, and after specific treatments, some bioactive materials were transformed into inert materials [67].

The biological performance of a porous apatite-mullite glass-ceramics, manufactured via the selective laser sintering (SLS) method, was investigated by Goodridge et al [165]. Laser-sintered A-M has shown similar cytotoxicity, in vitro bioactivity and in vivo results to cast A-M, indicating that the laser-sintering processing route does not alter the behavior of the material. The porous structure produced by SLS was seen by in vivo testing to be excellent for bone in-growth. However, the inability of the material to form apatite in vitro raised the concerns over the material's ability to prove bioactive in vivo, and further assessment is required to confirm whether this material is not bioactive or whether it is just not particularly suited for the characterization through SBF testing [165].

Author details

Petr Ptáček

Brno University of Technology, Czech Republic

References

[1] Meseguer S, Tena MA, Gargori C, Badenes JA, Llusar M, Monrós G. Structure and colour of cobalt ceramic pigments from phosphates. Ceramics International 2007;33(5) 843–849.

[2] Wagh AS. Introduction to Chemically Bonded Ceramics. Chemically Bonded Phosphate Ceramics, 2004. ISBN: 978-0-08-044505-2.

[3] Colorado HA, Hiel C, Hahn HT. Chemically bonded phosphate ceramics composites reinforced with graphite nanoplatelets. Composites Part A: Applied Science and Manufacturing 2011;42(4) 376–384.

[4] Dimitry SA. Characterization of reinforced chemically bonded ceramics. Cement and Concrete Composites 1991;13(4) 257–263.

[5] Yang L, Harink B, Habibovic P. Calcium phosphate ceramics with inorganic additives. Comprehensive Biomaterials 2011;1 299–312.

[6] Klammert U, Ignatius A, Wolfram U, Reuther T, Gbureck U. In vivo degradation of low temperature calcium and magnesium phosphate ceramics in a heterotopic model. Acta Biomaterialia 2011;7(9) 3469–3475.

[7] Chanda A, Dasgupta S, Bose S, Bandyopadhyay A. Microwave sintering of calcium phosphate ceramics. Materials Science and Engineering: C 2009;29(4) 1144–1149.

[8] Bandyopadhyay A, Withey EA, Moore J, Bose S. Influence of ZnO doping in calcium phosphate ceramics. Materials Science and Engineering: C 2007;27(1) 14–17.

[9] Formosa J, Chimenos JM, Lacasta AM, Niubó M. Interaction between low-grade magnesium oxide and boric acid in chemically bonded phosphate ceramics formulation. Ceramics International 2012;38(3) 2483–2493.

[10] Sahnoun RD, Bouaziz J. Sintering characteristics of kaolin in the presence of phosphoric acid binder. Ceramics International 2012;38(1) 1–7.

[11] Gardner LJ, Bernal SA, Walling SA, Corkhill CL, Provis JL, Hyatt NC. Characterisation of magnesium potassium phosphate cements blended with fly ash and ground granulated blast furnace slag. Cement and Concrete Research 2015;74 78–87.

[12] Liu Z, Qian G, Zhou J, Li C, Xu Y, Qin Z. Improvement of ground granulated blast furnace slag on stabilization/solidification of simulated mercury-doped wastes in chemically bonded phosphate ceramics. Journal of Hazardous Materials 2008;157(1) 146–153.

[13] Hermansson L. Nanostructural Bioceramics: Advances in Chemically Bonded Ceramics. CRC Press, 2014. ISBN: 978-9814463430

[14] Chen D, He L, Shang S. Study on aluminum phosphate binder and related Al_2O_3-SiC ceramic coating. Materials Science and Engineering: A 2003;348(1-2) 29–35.

[15] Hipedinger NE, Scian AN, Aglietti EF. Magnesia-ammonium phosphate-bonded cordierite refractory castables: Phase evolution on heating and mechanical properties. Cement and Concrete Research 2004;34(1) 157–164.

[16] Choi J, Um W, Choung S. Development of iron phosphate ceramic waste form to immobilize radioactive waste solution. Journal of Nuclear Materials 2014;452(1-3) 16–23.

[17] Metcalfe BL, Donald IW, Fong SK, Gerrard LA, Strachan DM, Scheele RD. Ageing of a phosphate ceramic used to immobilize chloride contaminated actinide waste. Journal of Nuclear Materials 2009;385(2) 485–488.

[18] Singh D, Mandalika VR, Parulekar SJ, Wagh AS. Magnesium potassium phosphate ceramic for ^{99}Tc immobilization. Journal of Nuclear Materials 2006;348(3) 272–282.

[19] Scheetz BE, Agrawal DK, Breval E, Roy R. Sodium zirconium phosphate (NZP) as a host structure for nuclear waste immobilization: A review. Waste Management 1994;14(6) 489–505.

[20] von Kobell F. Über den schillernden asbest von Reichenstein in Schlesien. Journal für Praktische Chemie 1834;2 297–298.

[21] Warren BE, Bragg WL. The structure of the chrysotile $H_4Mg_3Si_2O_9$. Zeitschrift für Kristallographie 1931;76 201–210.

[22] Falini G, Foresti E, Gazzano M, Gualtieri AF, Leoni M, Lesci IG, Roveri N. Tubular-shaped stoichiometric chrysotile nanocrystals. Chemistry — A European Journal 2004;10 3043–3049.

[23] Viani A, Gualtieri AF. Preparation of magnesium phosphate cement by recycling the product of thermal transformation of asbestos containing wastes. Cement and Concrete Research 2014;58 56–66.

[24] Ciullo PA. Industrial Minerals and Their Uses: A Handbook and Formulary. William Andrew, 1996. ISBN: 978-0815518082

[25] Clarke DB. Granitoid Rocks. International Studies in Economic Modelling — Volume 7. Topics in the Earth Sciences. Springer Science & Business Media, 1992. ISBN: 978-0412291708

[26] Ruh E. Concise Encyclopedia of Advanced Ceramic Materials. Advances in Materials Sciences and Engineering. Elsevier, 2012. ISBN: 978-0080983707

[27] Huggett LG. Refractories in the chemical industries. International Journal of Materials in Engineering Applications 1979;1(5) 280–294.

[28] Sadik C, El Amrani Iz-E, Albizane A. Recent advances in silica-alumina refractory: A review. Journal of Asian Ceramic Societies 2014;2(2) 83–96.

[29] Marghussian VK, Naghizadeh R. Chemical bonding of silicon carbide. Journal of the European Ceramic Society 1999;19(16) 2815–2821.

[30] Sujith SS, Kumar ASL, Mangalaraja RV, Mohamed AP, Ananthakumar S. Porous to dense $LaPO_4$ sintered ceramics for advanced refractories. Ceramics International 2014;40(9) 15121–15129.

[31] Souza TM, Luz AP, Santos T Jr, Gimenes DC, Miglioli MM, Correa AM, Pandolfelli VC. Phosphate chemical binder as an anti-hydration additive for Al_2O_3-MgO refractory castables. Ceramics International 2014;40(1) 1503–1512.

[32] Gale WF, Totemeier TC. Smithells Metals Reference Book. 8th ed., Butterworth-Heinemann, 2003. ISBN: 978-0080480961

[33] Luz AP, Gomes DT, Pandolfelli VC. High-alumina phosphate-bonded refractory castables: $Al(OH)_3$ sources and their effects. Ceramics International 2015;41(7) 9041–9050.

[34] García-Prieto A, Ramos-Lotito MD, Gutiérrez-Campos D, Pena P, Baudín C. Influence of microstructural characteristics on fracture toughness of refractory materials. Journal of the European Ceramic Society 2015;35(6) 1955–1970.

[35] Toy C, Whittemore OJ. Phosphate bonding with several calcined aluminas. Ceramics International 1989;15(3) 167–171.

[36] Hipedinger NE, Scian AN, Aglietti EF. Magnesia-phosphate bond for cold-setting cordierite-based refractories. Cement and Concrete Research 2002;32(5) 675–682.

[37] Lu W, Chung DDL. Oxidation protection of carbon materials by acid phosphate impregnation. Carbon 2002;40(8) 1249–1254.

[38] Smith BGN, Wright PS, Brown D. The Clinical Handling of Materials. 2nd ed., Oxford: Butterworth-Heinemann, 1994. ISBN: 978-0723610038

[39] Nicholson JW, Czarnecka B, Limanowska-Shaw H. A preliminary study of the effect of glass-ionomer and related dental cements on the pH of lactic acid storage solutions. Biomaterials 1999;20(2) 155–158.

[40] Liu Y, Yu Hai-Y. Does dental zinc phosphate cement really shrink in clinical applications? Medical Hypotheses 2009;73(2) 257–258.

[41] Schmalz G, Bindslev DA. Titul Biocompatibility of Dental Materials. Springer Science & Business Media, 2008. ISBN: 978-3540777823

[42] Paffenbarger GC, Sweeney WT, Isaacs A. Zinc phosphate cements: Physical properties and a specification. The Journal of the American Dental Association 1922;21(11) 1907–1924.

[43] Park C.-K, Silsbee MR, Roy DM. Setting reaction and resultant structure of zinc phosphate cement in various orthophosphoric acid cement-forming liquids. Cement and Concrete Research 1998;28(1) 141–150.

[44] Mitra SB. Dental cements: formulations and handling techniques. In: Curtis RV, Watson TF (Eds.), Dental Biomaterials. Elsevier, 2014. ISBN: 978-1845694241

[45] Jabri M, Mejdoubi E, El Gadi M, Hammouti B. Optimisation of hardness and setting time of dental zinc phosphate cement using a design of experiments. Arabian Journal of Chemistry 2012;5(3) 347–351.

[46] Wilson AD. The chemistry of dental cements. Chemical Society Reviews 1978;7(2) 265–296.

[47] Ramkumar N. Phosphate based oil well cements. ProQuest Dissertations and Theses; Thesis (Ph.D.)-University of Illinois at Chicago, 2005; Publication Number: AAI3199873; ISBN: 9780542467271; Source: Dissertation Abstracts International, Volume: 66-12, Section: B, page: 6863; 131 p.

[48] Kurdowski W. Cement and Concrete Chemistry. Springer Science & Business, 2014. ISBN: 978-9400779457

[49] Warner J. Practical Handbook of Grouting: Soil, Rock, and Structures. John Wiley & Sons, 2004. ISBN: 978-0471463030

[50] Ghosh SN. Cement and Concrete Science and Technology. Cement and Concrete Science & Technology — Part 1. Progress in Cement and Concrete. Thomas Telford, 1991. ISBN: 978-8185522005

[51] Wang F, Chen B, Pun EYB, Lin H. Alkaline aluminum phosphate glasses for thermal ion-exchanged optical waveguide. Optical Materials 2015;42 484–490.

[52] Saadaldin SA, Rizkalla AS. Synthesis and characterization of wollastonite glass-ceramics for dental implant applications. Dental Materials 2014;30(3) 364–371.

[53] Lewis M, Metcalf-Johansen J, Bell P. Crystallisation mechanisms in glass ceramics. Journal of Non-Crystalline Solids 1979;62 5–6.

[54] Stanton KT, O'Flynn KP, Kiernan S, Menuge J, Hill R. Spherulitic crystallization of apatite-mullite glass-ceramics: Mechanisms of formation and implications for fracture properties. Journal of Non-Crystalline Solids 2010;356(35-36) 1802–1813.

[55] Hill RG. Bioactive Glass-Ceramics, 181-186. Comprehensive Biomaterials, Volume 1. In: Ducheyne P (Ed.). Elsevier, 2011. ISBN: 978-0-08-055294-1

[56] Kamitakahara M, Ohtsuki C, Inada H, Tanihara M, Miyazaki T. Effect of ZnO addition on bioactive CaO-SiO_2-P_2O_5-CaF_2 glass-ceramics containing apatite and wollastonite. Acta Biomaterialia 2006;2(4) 467–471.

[57] Zhang Y, Santos JD. Microstructural characterization and in vitro apatite formation in CaO-P_2O_5-TiO_2-MgO-Na_2O glass-ceramics. Journal of the European Ceramic Society 2001;21(2) 169–175.

[58] Kishioka A, Hayashi M, Kinoshita M. Glass formation and crystallization in ternary phosphate systems containing Al_2O_3. Bulletin of the Chemical Society of Japan 1976;49(11) 3032–3036.

[59] Joseph K, Jolley K, Smith R. Iron phosphate glasses: Structure determination and displacement energy thresholds, using a fixed charge potential model. Journal of Non-Crystalline Solids 2015;411 137–144.

[60] Stefanovsky SV, Stefanovsky OI, Kadyko MI, Presniakov IA, Myasoedov BF. The effect of Fe_2O_3 substitution for Al_2O_3 on the phase composition and structure of sodium-aluminum-iron phosphate glasses. Journal of Non-Crystalline Solids 2015;425 138–145.

[61] Premila M, Rajaraman R, Abhaya S, Ravindran TR, Kamali K, Amarendra G, Sundar CS. Spectroscopic evidence of irreversible changes in cesium loaded iron phosphate glasses under pressure. Journal of Non-Crystalline Solids 2014;406 111–118.

[62] Broglia G, Mugoni C, Du J, Siligardi C, Montorsi M. Lithium vanado-phosphate glasses: Structure and dynamics properties studied by molecular dynamics simulations. Journal of Non-Crystalline Solids 2014;403 53–61.

[63] Das SS, Singh NP, Srivastava PK. Ion conducting phosphate glassy materials. Progress in Crystal Growth and Characterization of Materials 2009;55(3-4) 47–62.

[64] Kishore MS, Pralong V, Caignaert V, Varadaraju UV, Raveau B. Synthesis and electrochemical properties of a new vanadyl phosphate: $Li_4VO(PO_4)_2$. Electrochemistry Communications 2006;8(10) 1558–1562.

[65] Kokubo T. Bioactive glass ceramics: properties and applications. Biomaterials 1991;12(2) 155–163.

[66] Cannillo V, Pierli F, Sampath S, Siligardi C. Thermal and physical characterisation of apatite/wollastonite bioactive glass-ceramics. Journal of the European Ceramic Society 2009;29(4) 611–619.

[67] Cannillo V, Colmenares-Angulo J, Lusvarghi L, Pierli F, Sampath S. In vitro characterisation of plasma-sprayed apatite/wollastonite glass-ceramic biocoatings on titanium alloys. Journal of the European Ceramic Society 2009;29(9) 1665–1677.

[68] Liu X, Ding C, Chu PK. Mechanism of apatite formation on wollastonite coatings in simulated body fluids. Biomaterials 2004;25(10) 1755–1761.

[69] Magallanes-Perdomo M, Luklinska ZB, De Aza AH, Carrodeguas RG, De Aza S, Pena P. Bone-like forming ability of apatite-wollastonite glass ceramic. Journal of the European Ceramic Society 2011;31(9) 1549–1561.

[70] Kokubo T. A/W glass-ceramic: Processing and properties. Chapter 5. In: Hench LL (Ed.). An Introduction to Bioceramics. Advanced Series in Ceramics — Volume 1. World Scientific, 1993. ISBN: 978-9810214005.

[71] Kokubo T, Shigematsu M, Nagashima Y, Tashiro M, Nakamura T, Yamamuro T, Higash S. Apatite- and wollastonite-containing glass ceramics for prosthetic applications. Bulletin of the Institute of Chemistry Research of Kyoto University 1982;60 260–268.

[72] Ma J, Chen CZ, Wang DG, Shao X, Wang CZ, Zhang HM. Effect of MgO addition on the crystallization and in vitro bioactivity of glass ceramics in the CaO-MgO-SiO_2-P_2O_5 system. Ceramics International 2012;38(8) 6677–6684.

[73] Clifford A., Hill R. Apatite-mullite glass-ceramics. Journal of Non-Crystalline Solids 1996;196 346–351.

[74] Hill RG, O'Donnell MD, Law RV, Karpukhina N, Cochrane B, Tulyaganov DU. The early stages of nucleation and crystallisation of an apatite glass-ceramic: Evidence for nano-scale crystallization. Journal of Non-Crystalline Solids 2010;356(52-54) 2935–2941.

[75] Bernardo E, Colombo P, Cacciotti I, Bianco A, Bedini R, Pecci R, Pardun K, Treccani L, Rezwan K. Porous wollastonite-hydroxyapatite bioceramics from a preceramic polymer and micro- or nano-sized fillers. Journal of the European Ceramic Society 2012;32(2) 399–408.

[76] van't Hoen C, Rheinberger V, Höland W, Apel E. Crystallization of oxyapatite in glass-ceramics. Journal of the European Ceramic Society 2007;27(2-3) 1579–1584.

[77] Mahato N, Banerjee A, Gupta A, Omar S, Balani K. Progress in material selection for solid oxide fuel cell technology: A review. Progress in Materials Science 2015;72 141–337.

[78] Fergus J, Hui R, Li X, Wilkinson DP, Zhang J. Solid Oxide Fuel Cells: Materials Properties and Performance. Chemistry and Chemical Engineering. CRC Press, 2008. ISBN: 978-1420088847.

[79] Grove WR. On voltaic series and combination of gases by platinum. Philosophical Magazine Series 3 1839;14(86) 127–130.

[80] Camaratta M. Microstructural engineering of composite cathode systems for intermediate and low temperature solid oxide fuel cells, Ph.D. Thesis. Gainesville, Florida: University of Florida, 2007.

[81] Marrero-López D, Martín-Sedeño MC, Peña-Martínez J, Ruiz-Morales JC, Núñez P, Aranda MAG, Ramos-Barrado JR. Evaluation of apatite silicates as solid oxide fuel cell electrolytes. Journal of Power Sources 2010;195(9) 2496–2506.

[82] Islam MS, Tolchard JR, Slater PR. An apatite for fast oxide-ion conduction. Chemical Communications 2003;(13) 1486–1487.

[83] Tolchard JR, Islam MS, Slater PR. Defect chemistry and oxygen ion migration in the apatite-type materials $La_{9.33}Si_6O_{26}$ and $La_8Sr_2Si_6O_{26}$. Journal of Materials Chemistry 2003;13(8) 1956–1961.

[84] Zeng Y, Mao Pei-L, Jiang SP, Wu P, Zhang L, Wu P. Prediction of oxygen ion conduction from relative Coulomb electronic interactions in oxyapatites. Journal of Power Sources 2011;196(10) 4524–4532.

[85] Nakayama S, Higuchi Y, Sugawara M, Makiya A, Uematsu K, Sakamoto M. Fabrication of c-axis-oriented apatite-type polycrystalline $La_{10}Si_6O_{27}$ ceramic and its anisotropic oxide ionic conductivity. Ceramics International 2014;40(1) 1221–1224.

[86] Takeda N, Itagaki Y, Aono H, Sadaoka Y. Preparation and characterization of $Ln_{9.33+x/3}Si_{6-x}Al_xO_{26}$ (Ln = La, Nd and Sm) with apatite-type structure and its application to a potentiometric O_2 gas sensor. Sensors and Actuators B: Chemical 2006;115(1) 455–459.

[87] Tudorache F, Petrila I, Popa K, Catargiu AM. Electrical properties and humidity sensor characteristics of lead hydroxyapatite material. Applied Surface Science 2014;303 175–179.

[88] Owada H, Yamashita K, Umegaki T, Kanazawa T, Nagai M. Humidity-sensitivity of yttrium substituted apatite ceramics. Solid State Ionics 1989;35(3-4) 401–404.

[89] Nagai M, Nishino T, Saeki T. A new type of CO_2 gas sensor comprising porous hydroxyapatite ceramics. Sensors and Actuators 1988;15(2) 145–151.

[90] Phosphor system for improved efficacy lighting sources. Patent US 8866372 B2, 2011.

[91] Yu R, Xue N, Wang T, Zhao Z, Wang J, Hei Z, Li M, Noh HM, Jeong JH. Photoluminescence characteristics of high thermal stable fluorosilicate apatite $Ba_2Y_3(SiO_4)_3F$: Sm^{3+} orange-red emitting phosphor. Ceramics International 2015;41(4) 6030–6036.

[92] Liu Y, Wang Z, Zhong J, Pan F, Liang H, Xiao Z. Synthesis and photoluminescence properties of red-emitting phosphors $Ba_2Gd_8(SiO_4)_6O_2$:Eu^{3+}. Materials Letters 2014;129 130–133.

[93] Sokolnicki J, Zych E. Synthesis and spectroscopic investigations of $Sr_2Y_8(SiO_4)_6O_2$:Eu^{2+},Eu^{3+} phosphor for white LEDs. Journal of Luminescence 2015;158 65–69.

[94] Zhang F, Liu B. An intense red-emitting phosphor $Ca_3Gd_7(SiO_4)_5(PO_4)O_2$: Eu^{3+} for NUV-LEDs application. Journal of Alloys and Compounds 2012;542 276–279.

[95] Jeon YI, Bharat LK, Yu JS. White-light emission of $Ca_2La_8(GeO_4)_6O_2$: Tb^{3+}/Sm^{3+} nanocrystalline phosphors for solid-state lighting applications. Journal of Luminescence 2015;166 93–100.

[96] Liu H, Zhang Y, Liao L, Guo Q, Mei L. Synthesis, broad-band absorption and luminescence properties of blue-emitting phosphor $Sr_8La_2(PO_4)_6O_2$:Eu^{2+} for n-UV white-light-emitting diodes. Ceramics International 2014;40(8) 13709–13713.

[97] Roh Hee-S, Hur S, Song HJ, Park IJ, Yim DK, Kim Dong-W, Hong KS. Luminescence properties of $Ca_5(PO_4)_2SiO_4$:Eu^{2+} green phosphor for near UV-based white LED. Materials Letters 2012;70 37–39.

[98] Augustine RL. Heterogeneous Catalysis for the Synthetic Chemist. CRC Press, 1995. ISBN: 978-0824790219

[99] Gruselle M. Apatites: A new family of catalysts in organic synthesis. Journal of Organometallic Chemistry 2015. In press. DOI: 10.1016/j.jorganchem.2015.01.018

[100] Maaten B, Moussa J, Desmarets C, Gredin P, Beaunier P, Kanger T, Tõnsuaadu K, Villemin D, Gruselle M. Cu-modified hydroxy-apatite as catalyst for Glaser-Hay Csingle bondC homo-coupling reaction of terminal alkynes. Journal of Molecular Catalysis A: Chemical 2014;393 112–116.

[101] Li JJ. Name Reactions for Homologation, Part I. John Wiley & Sons, 2009. ISBN: 978-0470487013.

[102] Edition D. Apatite catalyst used to synthesise n-butanol from ethanol. Focus on Catalysts 2005;4 5–6.

[103] Cubberly WH, Bakerjian R. Tool and Manufacturing Engineers Handbook Desk Edition. Society of Manufacturing Engineers, 1989. ISBN: 978-0872633513

[104] Wang LK, Hung Yung-T, Shammas NK. Handbook of Advanced Industrial and Hazardous Wastes Treatment. Advances in Industrial and Hazardous Wastes Treatment. CRC Press, 2009. ISBN: 978-1420072228

[105] Su Hsiang-Y, Lin Chao-S. Effect of additives on the properties of phosphate conversion coating on electrogalvanized steel sheet. Corrosion Science 2014;83 137–146.

[106] Liu B, Zhang X, Gui-y Xiao, Lu Yu-p. Phosphate chemical conversion coatings on metallic substrates for biomedical application: A review. Materials Science and Engineering: C 2015;47 97–104.

[107] Perrin FX, Gigandet MP, Wery M, Pagetti J. Chromium phosphate conversion coatings on zinc electroplates: cathodic formation and characterization. Surface and Coatings Technology 1998;105(1-2) 135–140.

[108] Wopenka B, Pasteris JD. A mineralogical perspective on the apatite in bone. Materials Science and Engineering: C 2005;25(2) 131–143.

[109] López-Álvarez M, Rodríguez-Valencia C, Serra J, González P. Bio-inspired ceramics: promising scaffolds for bone tissue engineering. Procedia Engineering 2013;59 51–58.

[110] Abdel-Hameed SAM, Hessien MM, Azooz MA. Preparation and characterization of some ferromagnetic glass-ceramics contains high quantity of magnetite. Ceramics International 2009;35(4) 1539–1544.

[111] Matsumotoa T, Uddina MH, Ana SH, Arakawab K, Taguchib E, Nakahirac A, Okazakid M. Modulation of nanotube formation in apatite single crystal via organic molecule incorporation. Materials Chemistry and Physics 2011;128(3) 495–499.

[112] Nakano T, Kaibara K, Ishimoto T, Tabata Y, Umakoshi Y. Biological apatite (BAp) crystallographic orientation and texture as a new index for assessing the microstructure and function of bone regenerated by tissue engineering. Bone 2012;51(4) 741–747.

[113] Venkatesan J, Bhatnagar I, Manivasagan P, Kang Kyong-H, Kim Se-K. Alginate composites for bone tissue engineering: A review. International Journal of Biological Macromolecules 2015;72 269–281.

[114] Liu Y, Lim J, Teoh Swee-H. Review: Development of clinically relevant scaffolds for vascularised bone tissue engineering. Biotechnology Advances 2013;31(5) 688–705.

[115] Armentano I, Dottori M, Fortunati E, Mattioli S, Kenny JM. Biodegradable polymer matrix nanocomposites for tissue engineering: A review. Polymer Degradation and Stability 2010;95(11) 2126–2146.

[116] Nicholson JW. The Chemistry of Medical and Dental Materials. RSC Materials Monographs — Volume 3. Royal Society of Chemistry, 2002. ISBN: 978-0854045723

[117] Gómez-Morales J, Iafisco Mi, Delgado-López JM, Sarda S, Drouet C. Progress on the preparation of nanocrystalline apatites and surface characterization: Overview of fundamental and applied aspects. Progress in Crystal Growth and Characterization of Materials 2013;59(1) 1–46.

[118] Rey C, Combes C, Drouet C, Sfihi H, Barroug A. Physico-chemical properties of nanocrystalline apatites: Implications for biominerals and biomaterials. Materials Science and Engineering: C 2007;27(2) 198–205.

[119] Szymendera J. Bone Mineral Metabolism in Cancer. Recent Results in Cancer Research — Volume 27. Springer Science & Business Media, 2012. ISBN: 978-3642999789

[120] Hillson S. Teeth. Cambridge Manuals in Archaeology. 2nd ed., Cambridge University Press, 2005. ISBN: 978-1139444057

[121] Wilson RM, Elliot JC, Dowker SEP. Rietveld refinement of the crystallographic structure of human dental enamel apatites Sample: RHB-enamel. American Mineralogist 1999;84 1406–1414.

[122] Krivovichev SV. Titul Minerals as Advanced Materials I. Springer Science & Business Media, 2008. ISBN: 978-3540771234

[123] Jamuna-Thevi K, Daud NM, Kadir MRA, Hermawan H. The influence of new wet synthesis route on the morphology, crystallinity and thermal stability of multiple ions doped nanoapatite. Ceramics International 2014;40(1) 1001–1012.

[124] Delgado-López JM, Iafisco M, Rodríguez I, Tampieri A, Prat M, Gómez-Morales J. Crystallization of bioinspired citrate-functionalized nanoapatite with tailored carbonate content. Acta Biomaterialia 2012;8(9) 3491–3499.

[125] Gualtieri ML, Ma Romagnoli, Hanuskova M, Fabbri E, Gualtieri AF. Facile synthesis of B-type carbonated nanoapatite with tailored microstructure. Journal of Solid State Chemistry 2014;220 60–69.

[126] Xia Z, Yu X, Jiang X, Brody HD, Rowe DW, Wei M. Fabrication and characterization of biomimetic collagen-apatite scaffolds with tunable structures for bone tissue engineering. Acta Biomaterialia 2013;9(7) 7308–7319.

[127] Sader MS, Martins VCA, Gomez S, LeGeros RZ, Soares GA. Production and in vitro characterization of 3D porous scaffolds made of magnesium carbonate apatite (MCA)/ anionic collagen using a biomimetic approach. Materials Science and Engineering: C 2013;33(7) 4188–4196.

[128] Fricain JC, Schlaubitz S, Le Visage C, Arnault I, Derkaoui SM, Siadous R, Catros S, Lalande C, Bareille R, Renard M, Fabre T, Cornet S, Durand M, Léonard A, Sahraoui N, Letourneur D, Amédée J. A nano-hydroxyapatite — Pullulan/dextran polysaccharide composite macroporous material for bone tissue engineering. Biomaterials 2013;34(12) 2947–2959.

[129] Shoulders MD, Raines RT: Collagen structure and stability. Annual Review of Biochemistry 2009 ;78 929–958.

[130] Wahl DA, Czernuszka JT. Collagen-hydroxyapatite composites for hard tissue repair. European Cells and Materials 2006;11 43–56.

[131] Magne D, Pilet P, Weiss P, Daculsi G. Fourier transform infrared microspectroscopic investigation of the maturation of nonstoichiometric apatites in mineralized tissues: a horse dentin study. Bone 2001;29(6) 547–552.

[132] Li H, Guo Z, Xue B, Zhang Y, Huang W. Collagen modulating crystallization of apatite in a biomimetic gel system. Ceramics International 2011;37(7) 2305–2310.

[133] Su X, Sun K, Cui FZ, Landis WJ. Organization of apatite crystals in human woven bone. Bone 2003;32(2) 150–162.

[134] Okazaki M, Ohmae H, Hino T. Insolubilization of apatite-collagen composites by UV irradiation. Biomaterials 1989;10(8) 564–568.

[135] Okazakl M, Ohmae H, Takahashi J, Kimura H, Sakuda M. Insolubilized properties of UV-irradiated C03 apatite-collagen composites. Biomaterials 1990;11(8) 568–572.

[136] Müller FA, Müller L, Caillard D, Conforto E. Preferred growth orientation of biomimetic apatite crystals. Journal of Crystal Growth 2007;304(2) 464–471.

[137] Fernandez-Yague MA, Abbah SA, McNamara L, Zeugolis DI, Pandit A, Biggs MJ. Biomimetic approaches in bone tissue engineering: Integrating biological and physicomechanical strategies. Advanced Drug Delivery Reviews 2015;84 1–29.

[138] Chu CL, Pu YP, Yin LH, Chung CY, Yeung KWK, Chu PK. Biomimetic deposition process of an apatite coating on NiTi shape memory alloy. Materials Letters 2006;60(24) 3002–3006.

[139] Shi J, Ding C, Wu Y. Biomimetic apatite layers on plasma-sprayed titanium coatings after surface modification. Surface and Coatings Technology 2001;137(1) 97–103.

[140] Song Won-H, Jun Youn-K, Han Y, Hong Seong-H. Biomimetic apatite coatings on micro-arc oxidized titania. Biomaterials 2004;25(17) 3341–3349.

[141] Faure J, Balamurugan A, Benhayoune H, Torres P, Balossier G, Ferreira JMF. Morphological and chemical characterisation of biomimetic bone like apatite formation

on alkali treated Ti_6Al_4V titanium alloy. Materials Science and Engineering: C 2009;29(4) 1252–1257.

[142] Liu X, Fu RKY, Poon RWY, Chen P, Chu PK, Ding C. Biomimetic growth of apatite on hydrogen-implanted silicon. Biomaterials 2004;25(25) 5575–5581.

[143] Ye M, Mohanty P, Ghosh G. Biomimetic apatite-coated porous PVA scaffolds promote the growth of breast cancer cells. Materials Science and Engineering: C 2014;44 310–316.

[144] Kunze J, Müller L, Macak JM, Greil P, Schmuki P, Müller FA. Time-dependent growth of biomimetic apatite on anodic TiO_2 nanotubes. Electrochimica Acta 2008;53(23) 6995–7003.

[145] Rambo CR, Müller FA, Müller L, Sieber H, Hofmann I, Greil P. Biomimetic apatite coating on biomorphous alumina scaffolds. Materials Science and Engineering: C 2006;26(1) 92–99.

[146] Stefanic M, Krnel K, Pribosic I, Kosmac T. Rapid biomimetic deposition of octacalcium phosphate coatings on zirconia ceramics (Y-TZP) for dental implant applications. Applied Surface Science 2012;258(10) 4649–4656.

[147] Tavangarian F, Emadi R. Improving degradation rate and apatite formation ability of nanostructure forsterite. Ceramics International 2011;37(7) 2275–2280.

[148] Wu C, Chang J. Synthesis and apatite-formation ability of akermanite. Materials Letters 2004;58(19) 2415–2417.

[149] Múzquiz-Ramos EM, Cortés-Hernández DA, Escobedo-Bocardo J. Biomimetic apatite coating on magnetite particles. Materials Letters 2010;64(9) 1117–1119.

[150] Fujibayashi S, Neo M, Kim Hyun-M, Kokubo T, Nakamura T. A comparative study between in vivo bone ingrowth and in vitro apatite formation on Na_2O-CaO-SiO_2 glasses. Biomaterials 2003;24(8) 1349–1356.

[151] Berbecaru C, Alexandru HV, Ianculescu Ad, Popescu A, Socol G, Sima F, Mihailescu I. Bioglass thin films for biomimetic implants. Applied Surface Science 2009;255(10) 5476–5479.

[152] Bingel L, Groh D, Karpukhina N, Brauer DS. Influence of dissolution medium pH on ion release and apatite formation of Bioglass® 45S5. Materials Letters 2015;143 279–282.

[153] Gandolfi MG, Taddei P, Tinti A, De Stefano Dorigo E, Prati C. Alpha-TCP improves the apatite-formation ability of calcium-silicate hydraulic cement soaked in phosphate solutions. Materials Science and Engineering: C 2011;31(7) 1412–1422.

[154] Pangdaeng S, Sata V, Aguiar JB, Pacheco-Torgal F, Chindaprasirt P. Apatite formation on calcined kaolin-white Portland cement geopolymer. Materials Science and Engineering: C 2015;51 1–6.

[155] Akasaka T, Watari F, Sato Y, Tohji K. Apatite formation on carbon nanotubes. Materials Science and Engineering: C 2006;26(4) 675–678.

[156] Wu C, Chan J. Bonelike apatite formation on carbon microspheres. Materials Letters 2007;61(11-12) 2502–2505.

[157] Pan H, Zhao X, Darvell BW, Lu WW. Apatite-formation ability — Predictor of "bioactivity"? Acta Biomaterialia 2010;6(11) 4181–4188.

[158] Tien Wen-B, Chen Ming-T, Yao Pin-C. Effects of pH and temperature on microstructure and morphology of hydroxyapatite/collagen composites synthesized in vitro. Materials Science and Engineering: C 2012;32(7) 2096–2102.

[159] Wang J, Liu C. Biomimetic collagen/hydroxyapatite composite scaffolds: Fabrication and characterizations. Journal of Bionic Engineering 2014;11(4) 600–609.

[160] Wenpo F, Gaofeng L, Shuying F, Yuanming Q, Keyong T. Preparation and characterization of collagen-hydroxyapatite/pectin composite. International Journal of Biological Macromolecules 2015;74 218–223.

[161] Holt C, Lenton S, Nylander T, Sørensen ES, Teixeira SCM. Mineralisation of soft and hard tissues and the stability of biofluids. Journal of Structural Biology 2014;185(3) 383–396.

[162] Kakkar P, Verma S, Manjubala I, Madhan B. Development of keratin-chitosan-gelatin composite scaffold for soft tissue engineering. Materials Science and Engineering: C 2014;45 343–347.

[163] Sharabi M, Mandelberg Y, Benayahu D, Benayahu Y, Azem A, Haj-Ali R. A new class of bio-composite materials of unique collagen fibers. Journal of the Mechanical Behavior of Biomedical Materials 2014;36 71–81.

[164] Marghussian V. Nano-Glass Ceramics: Processing, Properties and Applications. Elsevier Science, 2015. ISBN: 9780323354325

[165] Goodridge RD, Wood DJ, Ohtsuki C, Dalgarno KW. Biological evaluation of an apatite-mullite glass-ceramic produced via selective laser sintering. Acta Biomaterialia 2007;3(2) 221–231.